Applied Energy 197 (2017) 132–150

Contents lists available at ScienceDirect

Applied Energy

journal homepage: www.elsevier.com/locate/apenergy

Effect of pitch angle on power performance and aerodynamics of a vertical axis wind turbine

Abdolrahim Rezaeiha [a,*], Ivo Kalkman [a], Bert Blocken [a,b]

[a] Building Physics and Services, Department of the Built Environment, Eindhoven University of Technology, P.O. Box 513, 5600 MB Eindhoven, The Netherlands
[b] Building Physics Section, Department of Civil Engineering, KU Leuven, Kasteelpark Arenberg 40 – Bus 2447, 3001 Leuven, Belgium

HIGHLIGHTS

- For the studied turbine, a small negative pitch angle $\beta = -2°$ increases turbine C_P for 6.6% compared to $\beta = 0°$.
- Fixed pitch angle can affect the instantaneous and averaged loading and power conversion for VAWTs.
- Adding a fixed bound circulation (fixed β) can change the strength of shed vortices and wake generation for VAWTs.
- Fixed pitch angle shifts the instantaneous moment (C_m) on turbine blades between the fore and aft halves.
- The shift in C_m proposes individual blade dynamic pitching as a promising power enhancement method for VAWTs.

ARTICLE INFO

Article history:
Received 1 January 2017
Received in revised form 20 March 2017
Accepted 31 March 2017

Keywords:
Vertical axis wind turbine (VAWT)
Pitch angle
Aerodynamic performance
Optimization
CFD
URANS

ABSTRACT

Due to growing interest in wind energy harvesting offshore as well as in the urban environment, vertical axis wind turbines (VAWTs) have recently received renewed interest. Their omni-directional capability makes them a very interesting option for use with the frequently varying wind directions typically encountered in the built environment while their scalability and low installation costs make them highly suitable for offshore wind farms. However, they require further performance optimization to become competitive with horizontal axis wind turbines (HAWTs) as they currently have a lower power coefficient (C_P). This can be attributed both to the complexity of the flow around VAWTs and the significantly smaller amount of research they have received. The pitch angle is a potential parameter to enhance the performance of VAWTs. The current study investigates the variations in loads and moments on the turbine as well as the experienced angle of attack, shed vorticity and boundary layer events (leading edge and trailing edge separation, laminar-to-turbulent transition) as a function of pitch angle using Computational Fluid Dynamics (CFD) calculations. Pitch angles of −7° to +3° are investigated using Unsteady Reynolds-Averaged Navier-Stokes (URANS) calculations while turbulence is modeled with the 4-equation transition SST model. The results show that a 6.6% increase in C_P can be achieved using a pitch angle of −2° at a tip speed ratio of 4. Additionally, it is found that a change in pitch angle shifts instantaneous loads and moments between upwind and downwind halves of the turbine. The shift in instantaneous moment during the revolution for various pitch angles suggests that dynamic pitching might be a very promising approach for further performance optimization.

1. Introduction

VAWTs have recently received growing interest for energy harvesting purposes offshore [1–3] as well as in the urban environment [4–6]. They offer several advantages over HAWTs: omni-directional operation (hence no need for a yaw control mechanism), lower manufacturing costs due to simple blade profile and shape (no twist or taper), lower installation and maintenance costs due to having the generator installed at ground level (or sea level in case of offshore application), good scalability, robustness and lower noise level due to lower operational tip speed ratios (λ) [7]. Early development of VAWTs in the 1970s–1980s [8] could not lead to competitive designs in terms of performance and lifetime compared to HAWTs [7,9], possibly due to insufficient understanding of the complex aerodynamics of VAWTs. Complexities which were later found to play an important in VAWT behavior and performance include temporal/

* Corresponding author.
E-mail address: a.rezaeiha@tue.nl (A. Rezaeiha).

http://dx.doi.org/10.1016/j.apenergy.2017.03.128
0306-2619/

Nomenclature

A	turbine swept area, $h \cdot d$ [m^2]
c	blade chord length [m]
C_d	sectional drag coefficient [–]
C_f	skin friction coefficient [–]
C_{Fn}	coefficient of instantaneous sectional normal force [–]
C_{Fx}	coefficient of instantaneous sectional force in x-direction [–]
C_{Fy}	coefficient of instantaneous sectional force in y-direction [–]
C_l	sectional lift coefficient [–]
C_m	instantaneous moment coefficient [–]
C_P	power coefficient [–]
C_T	thrust coefficient [–]
C_Y	coefficient of net force in y-direction [–]
CoP	pressure coefficient [–]
d	turbine diameter [m]
D	sectional drag force [N/m]
F_t	sectional tangential force [N/m]
F_n	sectional normal force [N/m]
F_s	safety factor [–]
F_x	sectional force in x-direction [N/m]
F_y	sectional force in y-direction [N/m]
h	turbine height [m]
k	turbulence kinetic energy [m^2/s^2]
K	reduced frequency [–]
L	sectional lift force [N/m]
M	moment [N m]
n	number of blades [–]
P	power [W]
q	dynamic pressure [Pa]
R	turbine radius [m]
Re	chord-based Reynolds number, $U_{exp} \cdot \rho \cdot c/\mu$ [–]
Re_θ	momentum-thickness Reynolds number [–]
t	time [s]
T	thrust force [N]
U_{exp}	experienced velocity [m/s]
U_{ind}	induced velocity [m/s]
U_∞	freestream velocity [m/s]
α	experienced angle of attack [°]
α_d	experienced angle of attack on downstroke (decreasing α) [°]
α_{geo}	geometrical angle of attack [°]
α_{ss}	static stall angle [°]
α_u	experienced angle of attack on upstroke (increasing α) [°]
β	blade pitch angle [°]
γ	intermittency [–]
Γ	circulation [m^2/s]
θ	azimuth angle [°]
λ	tip speed ratio, $\Omega \cdot R/U_\infty$ [–]
μ	dynamic viscosity of air [kg/m s]
φ	flow angle [°]
ρ	density of air [kg/m^3]
σ	solidity, $n \cdot c/d$ [–]
ω	specific dissipation rate [1/s]
Ω	rotational speed [rad/s]

azimuthal variations of bound vorticity on the blades [10,11], blade-wake interactions and 3D wake characteristics [12,13], dynamic stall [14,15] and flow curvature [16,17]. Better understanding of these effects is essential for optimization of VAWT performance [18]. Research activities focused on this topic have employed various techniques. These include low-fidelity modeling which are typically momentum-based models such as the double multiple streamtube model [7]. Potential flow, cascade, vorticity and vortex transport models [19–21] are among the moderate-fidelity inviscid methods. Viscous CFD simulation is a high-fidelity method [22–26] which can provide much insight into the complete flow field although the accuracy of the results is very much dependent on computational parameters such as the number of turbine revolutions before data sampling, domain size, grid layout and resolution, and other numerical settings [25–27]. Wind tunnel measurements [28–31] and field experiments [32] have also been utilized both to provide an understanding of the flow physics and to provide validation data for modeling methods. These methods have been used to improve the performance of VAWTs where both the effect of geometrical parameters such as airfoil shape [33–35], blade solidity [36], blade pitch angle [37] and turbine tower [38], and of operational characteristics such as tip speed ratio [39] and freestream turbulence intensity [40,41] have been studied.

Among the aforementioned parameters, blade pitch angle (β) is very promising for performance optimization of VAWTs since it is very simple to apply in practice and does not introduce high manufacturing, installation or maintenance costs. The effect of pitch angle for VAWTs was studied by several authors [37,42–45] using the Double Multiple Streamtube Model [7]. However, the inaccuracy of this low-fidelity model for the prediction of the complex aerodynamics and performance of VAWTs was highlighted by Simão Ferreira, et al. [20]. Simão Ferreira and Scheurich [11] employed the moderate-fidelity inviscid 2D panel and 3D vorticity transport models in order to investigate the effect of fixed pitch angle. The study investigated pitch angles of −3°, 0° and +3° (see Fig. 1) and reported that although a shift in the instantaneous loads and moments was observed between the upwind and downwind sides of the turbine, the effect of pitch angle on the average loading, C_P and C_T, was negligible. The effect of fixed pitch angle was studied using high-fidelity viscous CFD simulations by Hwang et al. [46], Chen and Kuo [47], Zhang et al. [48] and Bose et al. [49]. However, numerical settings employed in the work of Hwang et al. [46], Chen and Kuo [47] and Bose et al. [49] did not meet recently derived minimum requirements for accurate assessment of VAWT performance [27] while this information was not reported by Zhang et al. [48]. Shortcomings included a too small domain size (small distance between the turbine and the inlet and/or outlet, high blockage ratio), large azimuthal increment ($d\theta$) and a small number of revolutions of the turbine before data sampling.

The effect of fixed pitch angles −7°, −4°, −2°, −0.5°, +1° and +3° on C_P was studied by Klimas and Worstell [32] for a 5-m Darrieus VAWT in an open-field experiment where −2° was found to be the

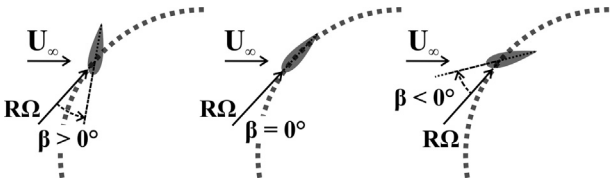

Fig. 1. Schematic showing the pitch angle for a VAWT blade.

optimum. The effect of the pitch angles −7.8°, −3.9°, 0°, +3.9° and 7.8° on C_P was studied by Fiedler and Tullis [50] for a high-solidity H-type VAWT in an open jet wind tunnel. The study concluded that a negative pitch angle provides optimal performance. Another experiment by Armstrong et al. [51] investigated an H-type 3-bladed VAWT with pitch angles −9° to +3° with steps of 3° in an open jet wind tunnel. A pitch angle of −3° was found to provide the optimal C_P for $\lambda = 2$. They also investigated a similar turbine with a helical blade and pitch angles of −5.5°, −3.5°, −1.5° and 2.5°, concluding that −3.5° provided the optimal C_P for $\lambda = 2$. The study also reported the separation areas using tufts on blades.

From the above it can be concluded that previous studies investigating the effect of fixed pitch angle have mainly focused on the value of the optimal pitch angle, considering only C_P values. However, variations of the instantaneous loads and moments are of paramount importance as they can highlight a potential for an optimum dynamic pitching for the turbine. Dynamic pitching has recently received interest as a promising solution for performance optimization [46,52,53]. In this case the pitch angle of each blade changes with azimuthal position. The optimum pitch angle distribution over a revolution can be determined from high-fidelity CFD simulations or experiments and will generally be different from the conventional cyclic pitching already investigated for VAWTs [54,55]. Furthermore, the fixed pitch angle studies performed so far have not investigated the effect of pitch angle on variations of angle of attack, dynamic loads on the airfoil, critical events in the boundary layer, pressure distribution on the blades and (apart from [11]) the wake generation of VAWTs.

In the current study a series of high-fidelity unsteady 2D Reynolds-averaged Navier-Stokes (URANS) viscous CFD simulations is performed, validated with experiments, in order to elucidate the effect of fixed pitch angle on instantaneous (such as C_m) and averaged loading (such as C_P and C_T) on a VAWT blade at a moderate tip speed ratio of 4. The study is performed in 2D since a comparison with 2.5D showed negligible (<1%) difference in C_P for a VAWT of similar operational and geometrical characteristics [27]. Moreover, the variation of experienced angle of attack on the blades for different pitch angles during the revolution is investigated. A deeper insight into the effect of pitch angle on the aerodynamics of the turbine is provided by comparing dynamic loads on the blades of a VAWT with static loads on a similar airfoil and discussing the change in critical boundary layer events: leading edge laminar separation, laminar-to-turbulent transition and trailing-edge turbulent separation. The findings are compared with those of pitching airfoils. Furthermore the pressure distributions over the blade at different azimuthal positions are compared for different pitch angles. Finally, a discussion on how the pitch angle influences the wake generation of the turbine is provided. It is believed that the insight provided by the present study can further clarify the effect of fixed pitch angle on the performance and aerodynamics of VAWTs and aid performance optimization of VAWTs in future studies on optimal dynamic pitching.

The novelty of the present study can be summarized as follows:

(1) In the existing literature the effect of pitch angle on VAWT performance has been investigated either using lower-fidelity modeling (compared to high-fidelity CFD) or the studies investigated only a few pitch angle values. As a result, current understanding of the way in which the pitch angle affects the fundamental flow processes underlying turbine performance is incomplete. The present study adds to the existing body of knowledge by employing high-fidelity URANS calculations, extensively validated against experimental data, to comprehensively investigate the influence of pitch angle on instantaneous and average loading of the turbine.
(2) The range of investigated pitch angles includes the optimum pitch angle which maximizes the turbine C_P together with 10 other values (5 higher and 5 lower than the optimum) with increments of 1°. This is a finer increment than used in previous studies, which provides a more detailed insight into how the aerodynamic performance changes for the neighboring pitch angles compared to the optimum one.
(3) In the existing literature mainly the effect of pitch angle on turbine averaged loading is investigated, while the present study provides a complete description of how the turbine instantaneous loading changes with pitch angle. Together with the fine pitch angle increments mentioned above this allows practical conclusions to be drawn for a next step in performance improvement of VAWTs, which is optimal dynamic pitching; a first estimate of the optimal pitch distribution can be derived from the provided distribution of instantaneous loads on the turbine for different pitch angles.
(4) The current study provides a comparison between the dynamic loading on turbine blades with that of the same static airfoil, which highlights the hysteresis effects even in the absence of dynamic stall. To the best of our knowledge this investigation has not been performed for VAWTs before. A comparison with literature on pitching airfoils is provided to highlight the similarities and differences.
(5) A thorough investigation is dedicated to elucidating the effect of pitch angle on the aerodynamics of VAWTs. The study investigates the influence of pitch angle on the variations of angle of attack, the boundary layer events on turbine blades (leading-edge laminar separation, laminar-to-turbulent transition and trailing-edge turbulent separation), the pressure coefficient and the strength of shed vortices, which to the authors' best knowledge has not been performed for such turbines in such detail before. The provided information can significantly support further optimization of VAWTs using optimal dynamic pitching or local flow control devices (e.g. turbulator, vortex generators, plasma actuators) to promote laminar-to-turbulent transition, delay flow separation or increase the airfoil circulation.

The outline of the paper is as follows: the geometrical and operational characteristics of the VAWT, the computational domain and grid, numerical settings and the method for calculation of the angle of attack are presented in Section 2. Section 3 discusses the sensitivity of the results to computational parameters: number of revolutions of the turbine before a converged solution is obtained (Section 3.1), grid resolution (Section 3.2) and azimuthal increment (3.3). Two validation studies on a 2-bladed and a 3-bladed VAWT are presented in Section 4. The effect of the pitch angle on the instantaneous and averaged loads and moments of the turbine (such as C_m, C_P and C_T) is discussed in Section 5. The aerodynamics of the turbine for various pitch angles are presented in Section 6. This section is subdivided into variations of the angle of attack (Section 6.2.1), dynamic loads on the blades (Section 6.2.2), pressure coefficient distributions (Section 6.2.3) and wake generation (Section 6.2.4). Section 7 contains a discussion on the correlations between the effect of pitch angle on loads and the aerodynamics. Conclusions are provided in Section 8.

2. Methodology

2.1. Static airfoil

In order to identify the static stall angle α_{ss} for the NACA0015 airfoil at a chord-based Reynolds number similar to that of the VAWT, a series of 2D CFD simulations are performed for a single

airfoil at different angles of attack. The results provide the static lift and drag coefficients, C_l and C_d, at the given Reynolds number for comparison with the dynamic values. This further helps to identify the effect of pitch angle on the dynamic loads, Section 6.2.2, and boundary layer events, Section 6.2.3.

The computational domain employed to simulate the static airfoil is a rectangle of 50c × 20c with the origin at the airfoil quarter chord (see Fig. 2a). The distance from the domain inlet and outlet to the origin is 10c and 40c, respectively, where the values are selected following the work of Kinzel et al. [56] where a minimum distance of 10c from the airfoil quarter chord $c/4$ to the domain inlet and outlet was shown to provide accurate results and minimize the effect of uncertainties in the boundary conditions on the results for a static airfoil.

The generated grid for the static airfoil consists of quadrilateral cells in the entire domain where a boundary layer grid is used on the airfoil walls. The grid near the airfoil is shown in Fig. 2b; enlarged views exhibiting close-ups of the grid near the airfoil leading edge and trailing edge are shown in Fig. 2c and d, respectively. A circular domain section is created around the airfoil (see Fig. 2a) in order to facilitate local grid refinement near the airfoil. The circle around the airfoil also simplifies the preprocessing phase for simulation of different angles of attack. A coarse grid with 800 nodes on the airfoil wall and a maximum y^+ below 2.8 is created. The grid is then systematically and uniformly refined with a factor of 1.41 (square root of 2) for Δx and Δy spacing everywhere, leading to a grid with approximately twice the total number of cells. The refinement is repeated twice in order to generate a medium and a fine grid (see Table 1) which are used to study the grid dependence of the results, as described in detail in Section 3.2.1. Refinement with a factor of 2 is commonly employed in grid convergence studies [57].

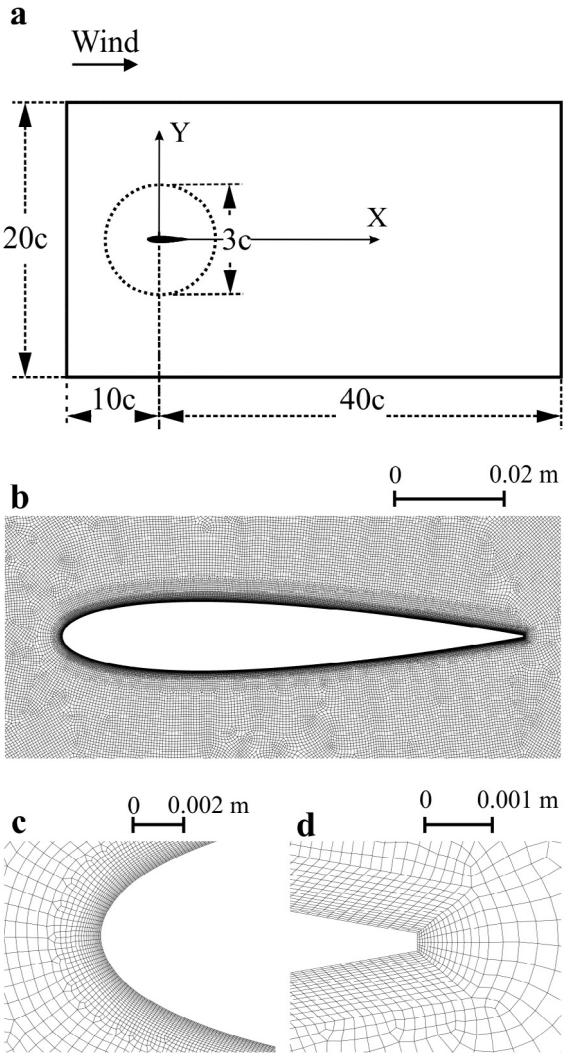

Fig. 2. (a) Computational domain (not to scale); (b) grid near the airfoil; (c) airfoil leading edge and (d) airfoil trailing edge for the static airfoil calculations.

The flow around the static airfoil is simulated for angles of attack from −9° to 15° using the finite volume-based commercial CFD software package ANSYS Fluent 16.1 [58]. The incompressible Reynolds-Averaged Navier-Stokes (RANS) equations are solved using the SIMPLE pressure-velocity coupling scheme, 2nd order pressure interpolation scheme and 2nd order upwind spatial discretization schemes. The gradient approximation is least squares cell based. A symmetry boundary condition is employed on the sides of the domain, along with a constant velocity inlet and an average zero gauge pressure outlet. A no-slip condition is used on the airfoil walls. The number of iterations for each steady-state simulation is 10,000 which ensures that all scaled residuals drop below 1×10^{-8}.

Turbulence is modeled using the 4-equation transition SST turbulence model [59]. This model couples the k-ω SST transport equations with two other equations for the intermittency (γ) and momentum-thickness Reynolds number (Re_θ) in order to provide a better prediction of transition onset in the boundary layer, which is deemed to be very important for airfoils and VAWTs since the flow strongly depends on the development of the boundary layer [60].

Inlet (and incident flow) mean velocities and turbulence intensities are 29.00 m/s (and 29.03 m/s) and 5% (and 4.91%), respectively. The inlet velocity corresponds to chord-based Re of 1.15×10^5. The incident value corresponds to the values in the same domain at the position of the airfoil leading edge ($\alpha = 0°$) when the airfoil is not present [61,62].

2.2. VAWT

2.2.1. Geometry and operational characteristics

A 3-bladed H-type low-solidity VAWT with geometrical and operational characteristics described in Table 2 is used in the current study. The turbine has a diameter and height of 1 m with a symmetric NACA0015 airfoil with a chord/radius ratio of 0.115 (solidity of 0.172) and a tip speed ratio of 4. An H-type VAWT rather than a Φ-type Darrius VAWT is considered for the current study mainly due to the aerodynamic and structural problems associated with Φ-type Darrius VAWTs [63] which has led to a research trend towards H-type turbines [64]. A 3-bladed rather than a 2-bladed VAWT is selected since it offers higher uniformity in the turbine output power as well as the turbine load variation [65]. In order to enable a clearer investigation of the effect of pitch angle on the aerodynamic performance of VAWTs a low solidity and a moderate tip speed ratio are selected to minimize the flow complexities. Specifically, a low solidity minimizes blade-wake interactions and consequent complexities; a moderate tip speed ratio avoids the occurrence of dynamic stall, as the experienced

Table 1
Details of the computational grids for the static airfoil.

Grid size	Cells	Maximum y^+ on airfoil
Coarse	216,221	2.8
Medium	577,557	2.3
Fine	864,884	1.4

Table 2
Geometrical and operational characteristics of the studied VAWT.

Parameter	Value
Number of blades, n [−]	3
Diameter, d [m]	1
Height, h [m]	1
Swept area, A [m^2]	1
Solidity, σ [−]	0.172
Chord/radius ratio, c/R [−]	0.115
Airfoil	NACA0015
Shaft diameter [m]	–
Tip speed ratio, λ [−]	4.0
Freestream velocity, U_∞ [m/s]	7.0
Rotational speed, Ω [rad/s]	56.0

angle of attack on the blades at zero pitch is below the static stall angle α_{ss} for the relevant chord-based Reynolds number [11,13].

The simulations are performed in two dimensions (2D) representing the midplane of a turbine. The 2D simulations are selected after a negligible difference (<1%) in power and thrust coefficients, C_P and C_T, was found between the 2.5D and 2D results for a VAWT with similar solidity and tip speed ratio [27]. An extensive verification study of the numerical settings used in the present simulations is provided in the same reference.

Freestream velocity and rotational speed are given in Table 2. The approach flow (at the domain inlet) and incident flow turbulence intensities are 5% and 4.42%, respectively. The incident value corresponds to the values in the same domain at the position of the turbine when the turbine is not present [61,62].

2.2.2. Computational domain and grid

In order to simulate the rotation of the turbine, the computational domain (Fig. 3) is divided into a rotating core with a diameter of 1.5 times the turbine diameter d and a fixed domain (30d length × 20d width) surrounding the rotating core. The interface between the rotating core and the fixed domain is a non-conformal interface with sliding grid to allow the rotation. The blockage ratio (which in 2D is defined as the ratio of turbine diameter to domain width) is 5%. A comprehensive systematic study by Rezaeiha et al. [27] performed for an H-type VAWT with a very similar solidity and tip speed ratio as employed in the current study showed that a blockage ratio of 5% ensures that the artificial acceleration of flow due to the presence of a symmetry condition on the side boundaries is insignificant and therefore has negligible impact on the calculated aerodynamic performance of the turbine; their results exhibited only a 0.2% change in calculated C_P when the blockage ratio decreased from 5% to 1.43%. Based on this, in the present study a blockage ratio of 5% is selected. The distances from the inlet and outlet of the domain to the center of rotation are 5d and 25d, respectively. The distance from the turbine center to the domain outlet, the domain width (blockage ratio) and the diameter of the rotating core employed in the current work respect the minimum requirements provided by Rezaeiha et al. [27] which resulted from a comprehensive systematic study on the domain size and azimuthal increment for a low-solidity VAWT operating at a moderate tip speed ratio of 4. A smaller distance from the turbine center to the domain inlet is used than is recommended in the same paper which can result in a 5.5% overestimation of turbine C_P. However, relative differences in turbine performance are expected to be much smaller.

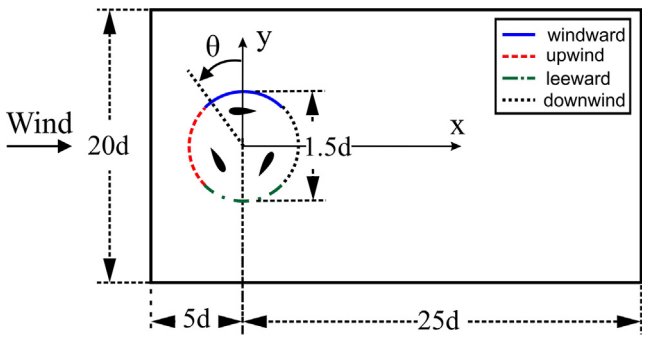

Fig. 3. Computational domain for the VAWT (not to scale).

Four quartiles are defined for the azimuthal angle θ following the work of Simão Ferreira [66]: upwind ($45° \leq \theta < 135°$), leeward ($135° \leq \theta < 225°$), downwind ($225° \leq \theta < 315°$) and windward ($315° \leq \theta < 45°$).

The computational grid for the VAWT (see Fig. 4) consists of quadrilateral cells and includes a boundary layer grid on the walls. The first cell height is such that the maximum y^+ in the simulations is ≤5 in order to resolve the viscous sublayer. Three grid resolutions are tested where the grid is uniformly refined; details are given in Table 3.

2.2.3. Numerical settings

The flow around the VAWT is simulated using the finite volume-based commercial CFD software package ANSYS Fluent 16.1 [58]. The incompressible Unsteady Reynolds-Averaged Navier-Stokes (URANS) equations are solved using the SIMPLE pressure-velocity coupling scheme and 2nd order spatial and temporal discretization schemes. These numerical settings are selected following the work of Rezaeiha et al. [27] and Balduzzi et al. [22] where the obtained results using these settings lead to a good agreement with experimental results. A symmetry boundary condition is employed on the sides of the domain, along with a constant velocity inlet and an average zero gauge pressure outlet. A no-slip condition is used on the airfoil walls. A domain interface is defined between the rotating core and the fixed domain. A periodic boundary condition is used at the top and bottom of the 2.5D domain. The initial conditions are based on a steady-state solution of the RANS equations. The azimuthal increment for the unsteady simulations of the turbine is 0.1°; this is equivalent to a time step of 3.11666×10^{-5} s. These values were obtained from a sensitivity analysis described in Section 3.3. The number of iterations per time step is set to 20 in order to ensure that all scaled residuals drop below 1×10^{-5}. Data sampling for the unsteady simulations is started after 20 revolutions of the turbine and continued for another 10 revolutions for averaging purposes; these values were found to be sufficient to ensure converged results are obtained (see Section 3.1). Turbulence in the transient simulations is modeled using the 4-equation transition SST model [59] in order to provide a better prediction of transition onset in the boundary layer as explained in Section 2.1.

2.2.4. Method for calculation of angle of attack

Calculation of the angle of attack for rotating blades using data from experiments or CFD simulations is a challenging task. This is due to the rotation of the blade which deviates the incoming flow as well as the bound circulation (vortex) around the blade that affects the flow field in the vicinity of the blade [67]. A schematic of the velocity triangle for a VAWT blade 2D cross-section is shown in Fig. 5a. Positive pitch angle (β) is defined as an inward rotation of the blade leading edge (towards the center of rotation of the turbine); this is shown with an arrow for the pitch angle and a grey airfoil.

The geometrical angle of attack (α_{geo}) for a VAWT can be defined from a geometrical relationship [7] (see Eq. (1)) assuming that the freestream velocity (U_∞) is not reduced by the turbine's thrust force (i.e. that the induced velocity (U_{ind}) is zero) and the turbine experi-

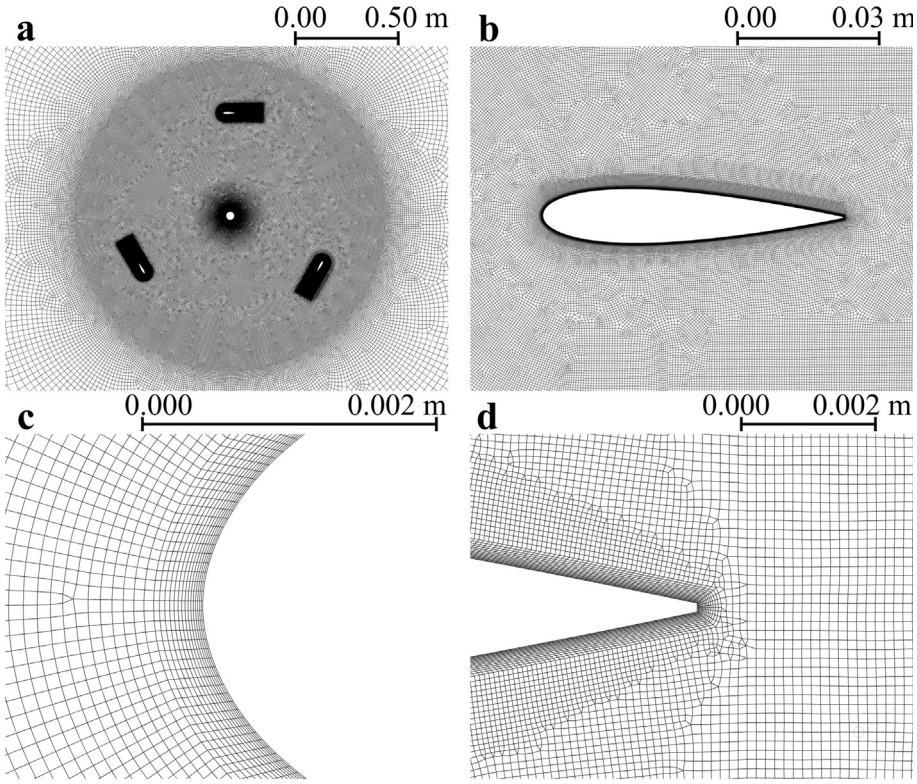

Fig. 4. Computational grid: (a) near the rotating core; (b) near the airfoil; (c) airfoil leading edge; (d) airfoil trailing edge.

Table 3
Details of the computational grids for VAWT.

Grid size	Cells	Maximum y^+ on blades
Coarse	289,397	5.0
Medium	573,481	2.8
Fine	991,185	2.0

ences the same incoming x-velocity in the downwind region as in the upwind region. However, in practice neither assumption is correct. Therefore, the experienced angle of attack (α) has a lower value and is defined as the angle between the experienced velocity (U_{exp}) and the airfoil chord line. The experienced velocity is calculated as the vector sum of freestream, rotational and induced velocities, as indicated in Fig. 5a. The value of α is the sum of the flow angle φ and pitch angle β, i.e. if $\beta = 0^\circ$ then $\alpha = \varphi$.

In the current study the induced velocity is determined using the sampled streamwise and lateral velocity components in monitor points on a circle with the same diameter as the turbine with a distance of 0.2d upwind at each azimuthal position (see Fig. 5b). This distance is found to be the closest distance where the local effect of bound circulation around the airfoil does not affect the sampled velocity appreciably. The values are averaged over 3600 time steps in one revolution.

$$\alpha_{geo} = \tan^{-1}\left(\frac{\sin\theta}{\cos\theta + \lambda}\right) \quad (1)$$

3. Sensitivity analysis

3.1. Revolution convergence analysis for VAWT

For unsteady calculations it is important to identify the number of time steps before a converged solution is obtained. For the simulation of wind turbines it is customary to express this in terms of the number of revolutions of the turbine before sampling the data. Calculations are performed for 30 revolutions of the turbine. The time history of power coefficient (C_P) and its relative change (with respect to the last revolution of the turbine) in normal and logarithmic scale are shown in Fig. 6. The change in C_P is very large during the first 10 revolutions of the turbine where data sampling would result in a significant overestimation of turbine performance. An asymptotic decrease is observed where C_P approaches the limit value at approximately 20 revolutions. At this point, the changes in C_P and C_T between two successive revolutions have dropped below 0.2% and 0.1%, respectively and the differences between the values at 20 revolutions and 30 revolutions are found to be less than 1.5%. Based on this sensitivity analysis, 20 revolutions of the turbine are considered sufficient to ensure that a statistically steady-state has been obtained and data sampling can be initiated. Subsequently data are sampled for 10 revolutions of the turbine. Instantaneous values presented in the paper correspond to the last revolution (revolution 30) while average values are calculated over all 10 revolutions.

3.2. Grid sensitivity analysis

3.2.1. Static airfoil

The grid sensitivity analysis is performed for the static airfoil at two angles of attack; i.e. $\alpha = 0^\circ$ and 12°; using the three different grids as detailed in Table 1. The pressure distributions over the static airfoil for the two angles of attack and the three grids are illustrated in Fig. 7. As shown in Fig. 7a, for $\alpha = 0^\circ$ the lines completely overlap. For $\alpha = 12^\circ$, where the flow is inherently more complex due to flow separation, the coarse grid seems not to have sufficient spatial resolution which results in oscillations in the pressure distribution over the blade for $0 < x/c < 0.2$. The oscillations disappear on refinement of the grid, and the medium and fine grid results

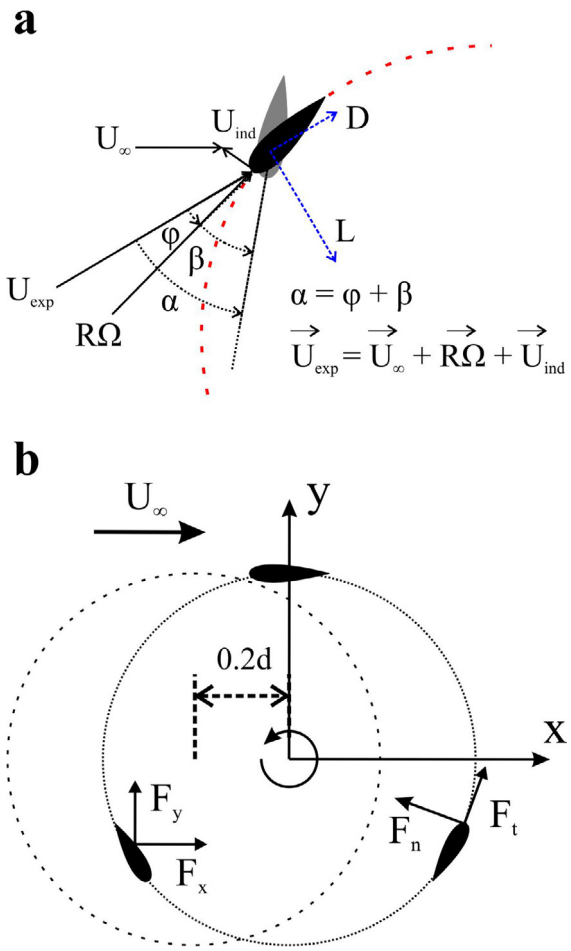

Fig. 5. (a) Velocity triangle for a VAWT blade; the grey airfoil shows positive pitch angle; (b) schematic of the VAWT showing the monitor points (dashed line) for velocity sampling for the calculation of α (not to scale).

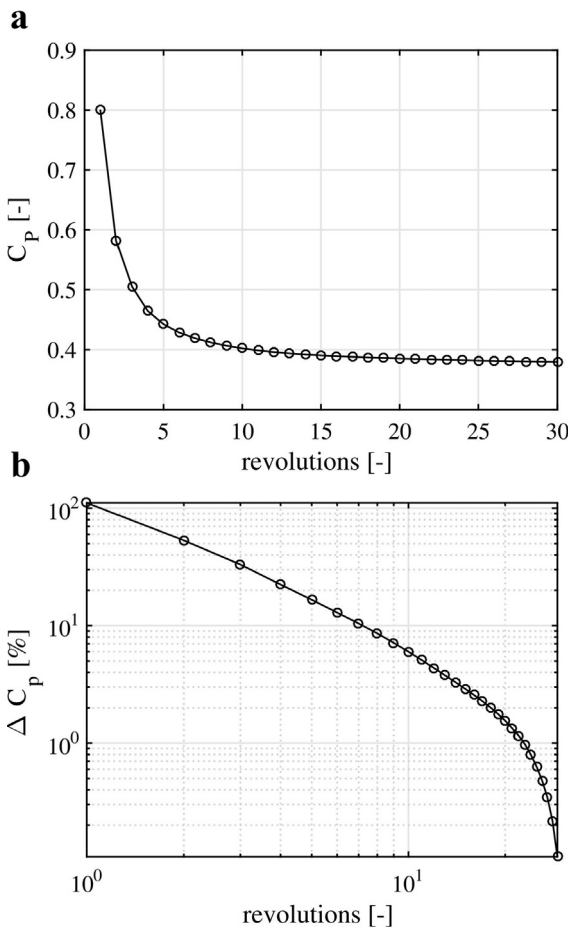

Fig. 6. History of power coefficients calculated summing the moment on all three blades (a) and its relative change with respect to the last revolution of the turbine in log-scale (b) for 30 revolutions. (dθ = 0.1°).

again overlap (Fig. 7b). The medium grid is selected as the maximum difference in C_l and C_d between the medium and fine grids for α = 0° and 12° is less than 1.1% and 1.9%, respectively.

3.2.2. VAWT

In order to check whether the grid for the VAWT is sufficiently fine a grid sensitivity analysis is carried out by performing calculations on the three grids described in Table 3. The grid resolution for these grids is systematically doubled in a uniform fashion using the criteria by Roache [57] as explained in Section 2.1; these criteria are widely used to quantify the uncertainties associated with the grid resolution for CFD studies. The current study uses the Grid Convergence Index (GCI) to assess the grid dependence of the results [57]. The GCI offers the merit of uniform reporting of the error for grid convergence studies. It also allows the user to estimate the solutions on grids with different resolutions and is defined based on a generalization of the Richardson Extrapolation [57,68].

Monitored quantities are the instantaneous moment coefficient C_m and the power and thrust coefficients, C_P and C_T, calculated using Eqs. (2) and (3), for the last turbine revolution.

$$C_P = \frac{P}{qU_\infty A} \tag{2}$$

$$C_T = \frac{T}{qA} \tag{3}$$

A plot of the instantaneous moment coefficient for one blade during the last turbine revolution versus azimuth (see Fig. 8) indicates a notable change when the grid is refined from coarse to medium grid. It is good to note that all the VAWT simulations performed include the full turbine with all three blades. The azimuthal increment used in the grid convergence study is 0.5°. Average and maximum absolute deviations of 0.005 and 0.026 are observed, respectively, resulting in a 2.16% change in C_P. The change in the instantaneous moment coefficient is negligible for further refinement from the medium to the fine grid, with average and maximum absolute deviations of 0.001 and 0.005, resulting in a less than 1% change in C_P. The GCI^{coarse} and GCI^{fine} for the coarse-medium grid pair, based on the C_P values using a safety factor (F_s) of 1.25, are determined to be 1.71×10^{-2} and 7.30×10^{-3}, respectively. Based on this grid sensitivity analysis the solution on the medium grid is found to be sufficiently independent of grid resolution. Therefore, the medium grid is selected for the rest of the calculations for the pitch study.

3.3. Azimuthal increment sensitivity analysis for VAWT

In order to investigate the sensitivity of the results to the azimuthal increment, simulations are performed with azimuthal increments from 1.0° to 0.1° for the turbine. The study shows that the refinement from 0.5° to 0.25° results in a relative change in C_P and C_T of 0.70% and 0.25%, respectively; for the refinement from

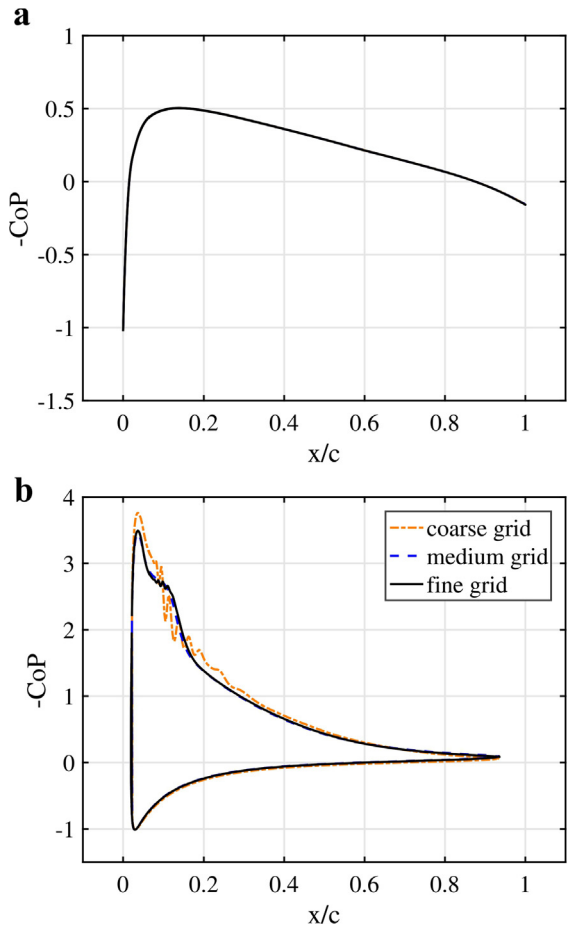

Fig. 7. Pressure coefficient (CoP) distribution over the static airfoil for (a) $\alpha = 0°$; (b) $\alpha = 12°$ for three different grids.

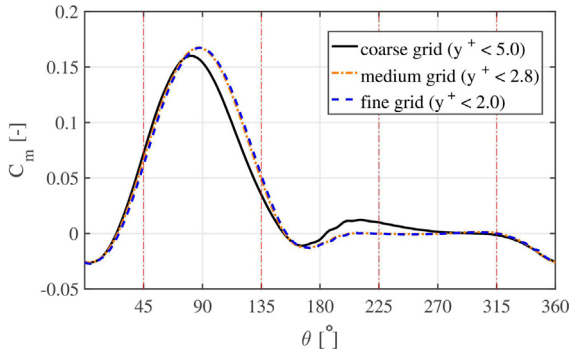

Fig. 8. Instantaneous moment coefficient for one blade for the last revolution versus azimuth for three different grids ($d\theta = 0.5°$).

0.25° to 0.1° these values are approximately 0.10%. The change in the instantaneous moment on the blade is also studied in order further investigate the sensitivity to the azimuthal increment (see Fig. 9). The results show a small difference in regions where the blade experiences higher angles of attack (further discussed in Section 6.2.1) and the downwind area. Therefore, as applying different pitch angles might result in higher variations of angle of attack, all subsequent calculations are performed using $d\theta = 0.1°$ in order to ensure good prediction of flow characteristics.

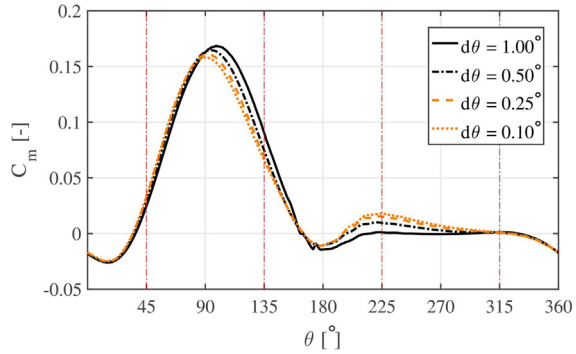

Fig. 9. Instantaneous moment coefficient for one blade for the last revolution versus azimuth for various azimuthal increments.

4. Validation study

In order to ensure the accuracy of the CFD results obtained in the present work two validation studies are discussed which employ the same numerical settings used here (see Section 2.2.3). The first extensive validation study performed in our group, presented in detail by Rezaeiha et al. [27], considers a 2-bladed H-type VAWT with a symmetric NACA0018 airfoil, a solidity of 0.12, a diameter of 1 m, and operating at a tip speed ratio of 4.5 with a freestream velocity of 9.3 m/s. The study compares the streamwise and lateral velocities in the turbine near wake against experimental data by Tescione et al. [13] at different downstream locations $2 \leq x/R \leq 4$. The average deviation from the experimental results for the streamwise and lateral velocities were below 16.4% and 2.9%, respectively. A comprehensive explanation of the possible reasons for the observed deviation is provided in [27] which for brevity is not repeated here.

The second validation study investigates a 3-bladed H-type VAWT with a symmetric NACA0021 airfoil, a solidity of 0.25 and a diameter of 1.03 m, operating at different tip speed ratios from 1.43 to 3.29 with a freestream velocity of 9 m/s. The computational domain and boundary conditions are the same as described in Section 2.2.2 except the distance from turbine center to the inlet, which is increased to 10d following recommendations by Rezaeiha et al. [27]. The computational grid is very similar to the grid shown in Fig. 4 and consists of 572,412 cells. The study compares the calculated turbine power coefficient C_P against the measured C_P values by Castelli et al. [69] for different tip speed ratios. As shown in Fig. 10 a good agreement is observed between the CFD results and experimental data. The following observations regarding the comparison can be made:

- The CFD results replicate the trend of change in C_P with tip speed ratio reasonably well although quantitative differences are observed for both low and high tip speed ratios.
- The present results exhibit much better agreement with experimental data than CFD results obtained by Castelli et al. [69]. The lower observed discrepancies can be attributed to the fact that the current study fully respects the guidelines provided by Rezaeiha et al. [27] for accurate CFD simulation of VAWT; violation of those minimum requirements for the number of turbine revolutions before data sampling, domain size and azimuthal increment were shown to lead to potentially large errors in the predicted turbine C_P.
- For moderate to high tip speed ratios there is an overestimation of calculated C_P. This can be partly associated to the fact that the blade tip losses are not present in 2D CFD. Another possible reason is the geometrical simplification and 2D modeling in the CFD analysis, e.g. the blade spokes and connecting struts to

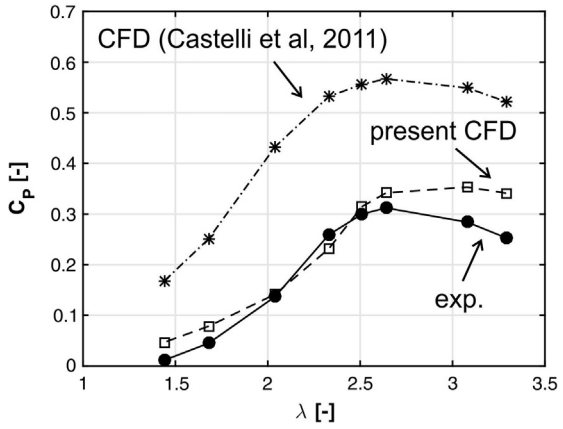

Fig. 10. Comparison of calculated power coefficient against experimental and numerical data by Castelli et al. [69].

the turbine tower result in considerable drag and reduce the turbine performance in the wind tunnel measurement while they are absent in the CFD simulations.

- For low to moderate tip speed ratios (where dynamic stall is present [14]) a similar overestimation in calculated C_P (compared to measured values) due to the geometrical simplifications is foreseen. The absence of such an overestimation for moderate tip speed ratios might suggest that the CFD results tend to underpredict the measured C_P at these operating conditions which cancels out the foreseen overestimation due to the geometrical simplifications. Such an underprediction might be associated with the inability of 2D URANS to accurately simulate the inherent 3D flow complexities associated with dynamic stall and blade-wake interactions.
- Uncertainties in the experimental data also might contribute to the observed discrepancy. Turbulence intensity is not reported in the experiment, and the reported freestream velocity and measured C_P values were not corrected for the blockage in the tunnel (approximately 10%). Furthermore the turbine blades surface smoothness is not clearly mentioned.

Based on the aforementioned discussions for the 2 validation studies the present CFD results are believed to provide a reasonable prediction of experimental data. The whole-domain flow field information obtained in these studies is complementary to such experiments and provides further understanding of the aerodynamic performance of VAWTs.

5. Loads and moments

5.1. Static airfoil

The C_l-α curve and pressure coefficient distributions are shown in Fig. 11. The lift coefficient C_l does not experience a sudden drop after the static stall angle α_{ss} (Fig. 11a). The soft stall of NACA0015 airfoil at the studied Re is a result of a gradual upstream movement of the trailing edge separation (see Section 6.1) which distinguishes the stall behavior from the thinner symmetric airfoils, such as NACA0012; where a sharp stall (as a result of bubble bursting) at similar Re is reported [70].

The static stall angle α_{ss} is found to be 12.8° for the given Reynolds number which is 1.15×10^5. The pressure coefficient distribution over the airfoil at different α is shown in Fig. 11b. The soft stall of the airfoil can also be predicted from the pressure distributions where at high angles of attack post-stall, e.g. $\alpha = 14°$, near the

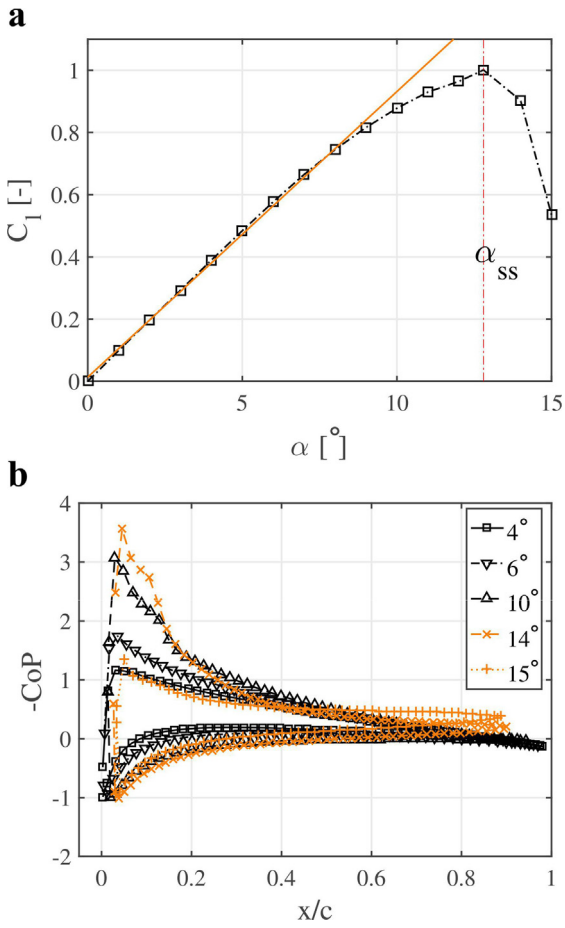

Fig. 11. Static airfoil data for a NACA0015 airfoil at $Re = 1.15 \times 10^5$: (a) C_l-α curve; (b) pressure coefficient (CoP) over the airfoil for different α.

leading edge (x/c < 0.15) there is still more negative pressure on the suction side compared to $\alpha = 10°$ which shows that the trailing edge separation has not yet reached this upstream location at this α. The airfoil experiences deep stall at $\alpha = 15°$. The pressure distributions can help to identify the laminar separation point and transition onset which will be elaborated in Section 6.1.

It is important to note that the results for the static airfoil case are solely presented here for comparison with the dynamic values obtained for a turbine blade in the VAWT. As the generated turbine power is directly related to the tangential force on blades, and the tangential force is calculated using only the blade lift and drag forces, the airfoil moment (around the aerodynamic center) is not investigated/presented here. It will be very important for studies which intend to analyze the structural loads and fatigue damage on the struts connecting the blade to the turbine tower, and will also play an important role for studies aiming to investigate the effect of blade structural vibrations on the aerodynamic performance of the turbine. However, these two important aspects are beyond the scope of the present study.

5.2. VAWT

Variations of the instantaneous moment coefficient versus azimuth for the VAWT for different pitch angles (see Fig. 12a) show that positive pitch angles (β) result in a higher moment coefficient only in a small part of the windward quartile and half of the upwind quartile ($25° \leq \theta \leq 90°$) while negative β can benefit the turbine over most of the revolution ($0° \leq \theta < 25°$ and

$90° < \theta \leq 360°$). In the region where positive β is helpful, the difference in C_m corresponding to β = +2° and +3° is very small. Comparing the instantaneous moment coefficients for β = +2° and +3°, the maximum value of C_m for β = +2° is 0.159 occurring at an azimuthal position of 83°, while the maximum value of C_m for β = +3° is 0.156 which occurs at an azimuthal position of 76°. Increasing β from +2° to +3° therefore reduces the magnitude of the maximum value of C_m while the maximum also occurs earlier in the revolution. In addition, the drop observed in C_m for $76° < \theta < 121°$ suggests that the pitch value causes the blade to experience deep stall for these azimuthal angles. The occurrence of stall for β = +3° is confirmed in Section 6.2.1 where the results reveal that the angle of attack exceeds the airfoil static stall angle. As increasing the pitch angle to a more positive value directly increases the angle of attack (see Section 6.2.1) it will result in an earlier stall on the blades and a greater power loss in the turbine. Therefore, as the focus of the present study is to investigate the effect of the pitch angle for the purpose of improvement of the aerodynamic performance of VAWTs, higher pitch angles β > +3° are not considered in the current study.

In the region where negative β is helpful a small negative value of β = −2° is optimal during half of the upwind and leeward quartiles ($90° < \theta < 160°$), while a large negative value of β = −6° is optimal during another half of the revolution (downwind quartile and half of the leeward and windward quartiles). Moreover, a more negative value of β = −7° reduces the moment in this region, implying that even more negative β will not be helpful: these are therefore not investigated. The reduction in moment at this β value is due to increased flow separation on the blade at β = −7° in the downwind quartile, where higher angles of attack are experienced.

It is also observed that changing β shifts the moment of the turbine between fore ($0° \leq \theta \leq 180°$) and aft ($180° < \theta < 360°$) halves of the revolution. This is in agreement with the findings of Simão Ferreira and Scheurich [11] where a similar shift is reported. This shift occurs from the first half of the upwind quartile ($45° < \theta < 90°$) to the downwind and part of the windward quartile. The change in β results in the least effect in the leeward quartile.

Having discussed the effect of pitch angle on the instantaneous moment on the blades, the C_P of the turbine as a representative of the average moment of the rotor during one revolution is calculated using Eq. (2). In order to find an optimum fixed pitch angle, C_P and the relative change in C_P with respect to zero pitch for different pitch angles show that the optimum pitch angle is −2° where a 6.6% increase in C_P is obtained compared to zero pitch angle (see Fig. 13a). A similar trend is also observed in wind tunnel measurements [32,50,51] where a performance enhancement for negative pitch angle and a performance drop for positive pitch angle are reported. The current finding is in contrast to the results of the inviscid study by Simão Ferreira and Scheurich [11] where they reported a negligible effect of pitch angle on C_P. This is an important result as introducing a fixed pitch angle is very simple from a practical point of view. Fig. 13a also shows the effect of stall for β = +3° with a dramatic reduction of 66.5% in C_P compared to zero pitch.

Variations of the instantaneous x-force coefficient (C_{Fx}) versus azimuth are also compared (see Fig. 12b) for different values of β.

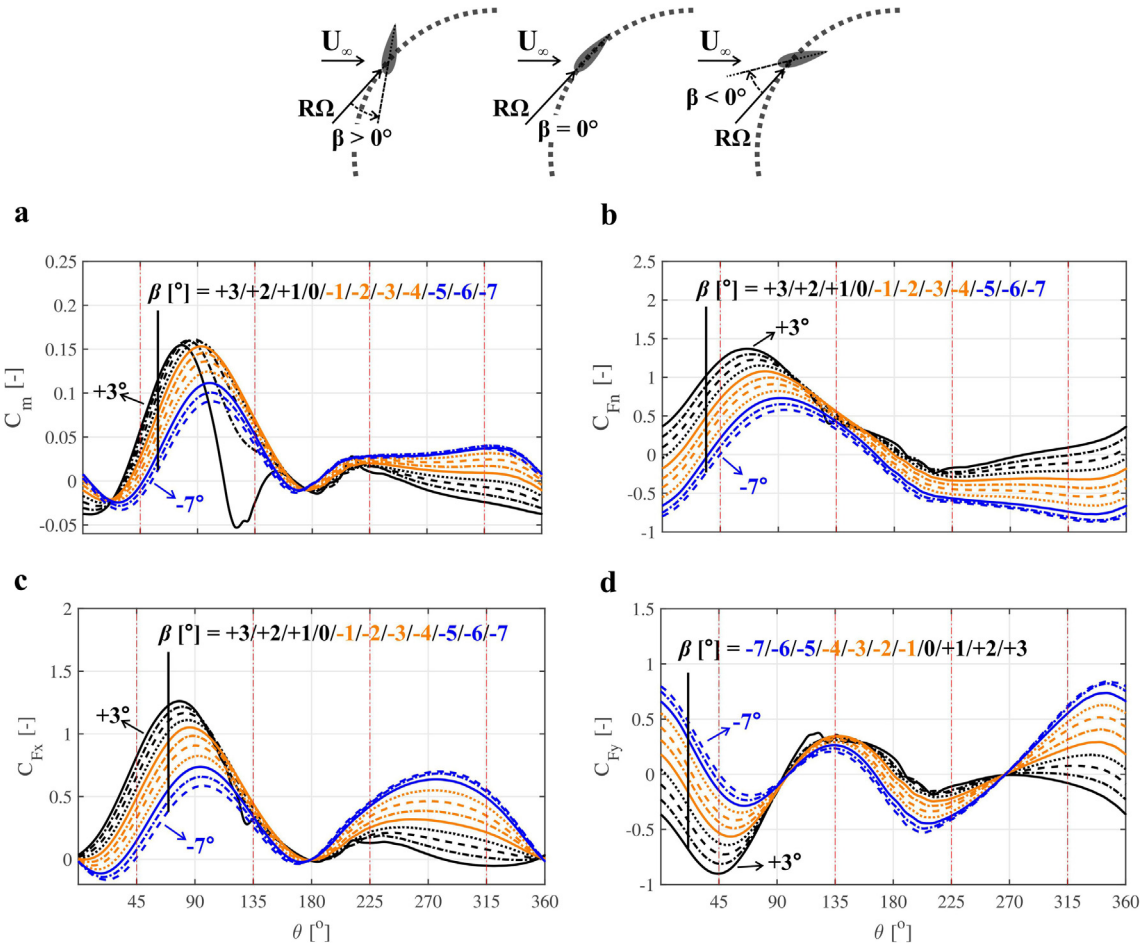

Fig. 12. Instantaneous load and moment coefficients for one blade during the last revolution versus azimuth at different pitch angles: (a) moment; (b) normal force; c) x-force; d) y-force.

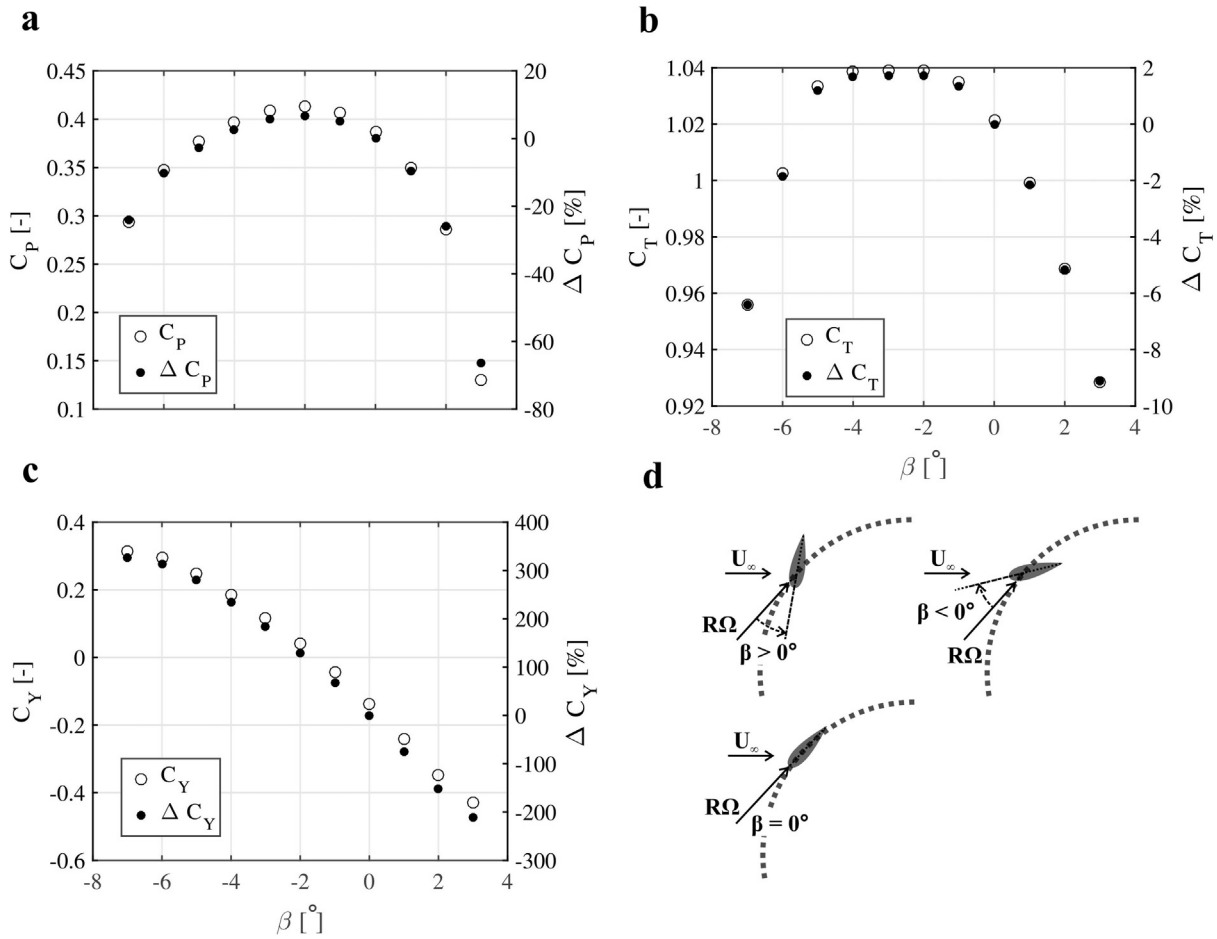

Fig. 13. Coefficients of (a) power, (b) thrust, (c) lateral force and their relative change to β = 0° versus pitch angle for the last revolution. (d) A schematic showing a blade with positive pitch angle.

Similar to the instantaneous moment on the blade (Fig. 12a), changing the pitch angle results in a shift in the instantaneous x-force (thrust force) between fore ($0° \leq \theta \leq 180°$) and aft ($180° < \theta < 360°$) halves of the revolution. This shift in x-force is also reported by Simão Ferreira and Scheurich [11]. The trend is very similar to that of C_m, however, a difference is also observed: within the studied range the more positive β results in higher C_{FX} for $0° \leq \theta \leq 180°$ while the more negative β yields higher C_{Fx} for $180° < \theta < 360°$ for all values considered. The decrease in C_m from $\beta = -6°$ to $\beta = -7°$ is not observed for C_{Fx}.

The thrust coefficient C_T, which is representative of the average streamwise loading on the turbine during one revolution, shows the same optimum $\beta = -2°$ found for C_P (see Fig. 13b) while the difference with $\beta = -3°$ and $-4°$ is negligible. This is in contrast with findings by Simão Ferreira and Scheurich [11] who concluded that pitch angle has a negligible effect on C_T. The relative change in C_T with β is found to be smaller than for C_P. C_T at the optimum value of $\beta = -2°$ is approximately 2% higher than at $\beta = 0°$. The higher value of C_T at the optimum fixed pitch angle also confirms that the turbine is extracting more energy from the incoming flow, resulting in a higher C_P. Moreover, the stall on the blade at $\beta = +3°$ affects the thrust force less than it does the moment. This is apparent from both C_{Fx} (Fig. 12b) and C_T (Fig. 13b), although the ripples in these curves in the range $90° < \theta < 160°$ indicate unsteadiness in the instantaneous x-force due to stalled flow on the blade. The smaller effect of stall on C_T is consistent with the lower sensitivity of thrust force to pitch angle compared to power.

The effect of fixed pitch angle is different for the normal force on the blades where increasing/decreasing the value of β is found to result in a higher/lower coefficient of normal force (C_{Fn}) almost throughout the revolution (see Fig. 12c). This difference is also observed by Simão Ferreira and Scheurich [11]. The effect of the stalled flow at $\beta = +3°$ is again apparent for $90° < \theta < 160°$.

The variations of the instantaneous y-force coefficient (C_{Fy}) versus azimuth for different β show that the shift in the y-force with changing β is between the top ($270° < \theta < 360$ and $0° \leq \theta < 90°$) and bottom ($90° \leq \theta \leq 270°$) halves of the revolution: see Fig. 12d. This is in contrast with the shift between fore and aft halves of the revolution observed for C_m and C_{FX}. The influence of unsteadiness due to the stalled flow on the blade for $\beta = +3°$ is again apparent as ripples in the instantaneous y-force for $90° < \theta < 160°$.

The net lateral force (C_Y), calculated using Eq. (4), is representative of the average lateral loading on the turbine during one revolution. C_Y shows the net y-force exerted by the flow on the blades as a result of which the flow receives the same force in the opposite direction. Therefore, $C_Y < 0$ means the turbine wake is skewed towards the windward side due to the net y-force from the blades; the reverse applies for $C_Y > 0$. The variations of C_Y with β show that the turbine wake is asymmetric towards the windward side for $\beta = 0°$ (see Fig. 13c), in agreement with experimental results of Tescione et al. [13]. It is observed that the more positive β deflects the wake more in the windward direction while the more negative β deflects it more in the leeward direction. Interestingly, it is observed that the optimum β results in approximately a symmetric wake where $C_Y \approx 0$.

$$C_Y = \frac{\Omega \int F_y dt}{2\pi q A} \quad (4)$$

The aforementioned discussions highlight the importance of turbine instantaneous loading as well as average loading. Therefore, in contrast with current common practice it is recommended that in both numerical and experimental research on VAWTs both instantaneous and averaged loading are reported in order to provide a thorough basis for comparative studies.

6. Aerodynamics

6.1. Static airfoil

Boundary layer event locations and separation bubble length for the static NACA0015 airfoil are shown in Fig. 14. The separation point corresponds to the point of vanishing wall shear in the boundary layer on the suction side where reverse flow is also observed [71]. The transition point corresponds to the sudden peak in the turbulent viscosity ratio in the boundary layer on the suction side where a sudden increase in the pressure coefficient is also observed [72]. It can be seen that the leading edge laminar separation point, the laminar-to-turbulent transition location and the trailing edge turbulent transition location move upstream with increasing α while having different slopes (Fig. 14a). This is in agreement with the trend observed in experimental data for a thinner NACA0012 airfoil [70]. The bubble length is found to increase slightly with increasing α (Fig. 14b). This is in contrast with the trend found for the thinner NACA0012 airfoil [70]. This might be due to the different stalling behavior for the two airfoils: the NACA0015 is found to exhibit trailing edge static stall where with increasing α, the turbulent separation location gradually moves upstream towards the leading edge until finally the flow fully separates on the suction side. Therefore, the lift coefficient C_l does not experience a sudden drop after the static stall angle α_{ss} (Fig. 11a). On the other hand the static stall behavior for the NACA0012 airfoil is typical of thin airfoils, a leading edge stall due to bubble bursting [70].

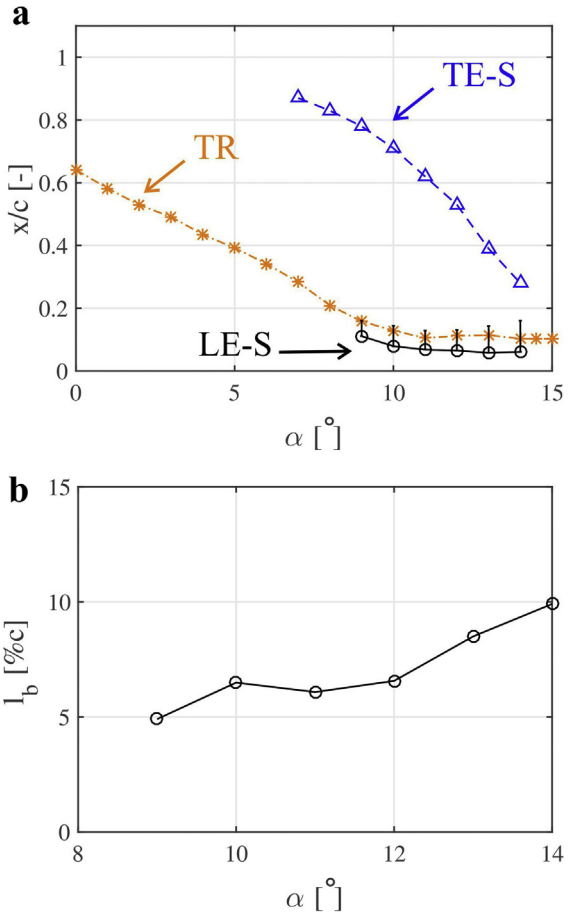

Fig. 14. Static airfoil data for a NACA0015 airfoil at $Re = 1.15 \times 10^5$: (a) critical flow points: LE-S, leading edge laminar separation (bar showing the laminar separation bubble length); TR, laminar-to-turbulent transition; TE-S, trailing edge turbulent separation; (b) laminar separation bubble length for different α.

6.2. VAWT

6.2.1. Angle of attack during the revolution

Two sources of flow unsteadiness are identified for a VAWT: (1) variations in the experienced angle of attack (α) for the blades during each revolution (see Fig. 15) and (2) variations in the experienced velocity (and local Reynolds number) by the blades (see Fig. 16), where the former is also a function of the latter. These two factors, which are also present for a pitching airfoil with time-dependent incoming flow, result in different loads on the unsteady airfoil of a VAWT compared to the static one and are known to create a hysteresis effect on the dynamic loads [71]. However, it has been found that they can have an opposite effect on critical boundary layer events: upward (downward) pitching of the airfoil is known to delay (promote) separation while variation in the incoming flow direction is known to promote separation [71]. This will be further discussed in Section 6.2.2 in order to identify the dominant effect for the VAWT.

Variations of α versus azimuth for different pitch angles β provide further insight into the variations of loads and moments on the blades. The study shows (see Fig. 15) that more positive (negative) β results in higher (lower) α throughout the revolution. Moreover, the values of α for $\beta = +3°$, $+2°$ (and $-7°$) exceed the static stall angle α_{ss} of $\pm 12.8°$ (see Section 6.1) in the upwind (downwind) quartiles. The occurrence of stall is also observed in the variations of C_m for $\beta = +3°$, as discussed in Section 5. However, for $\beta = +2°$ and $-7°$ the stall does not occur although $\alpha > \pm\alpha_{ss}$. This is due to the higher resistance of the boundary layer to separation during the upstroke (increasing absolute angle of attack α_u) for an unsteady airfoil compared to the static airfoil [71], which delays the stall. The oscillations observed in α on the downwind side

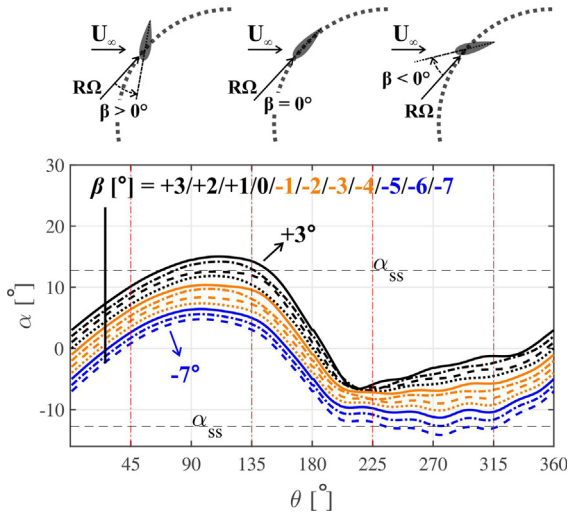

Fig. 15. Experienced angle of attack versus azimuth for different pitch angles; horizontal dashed line shows the static stall angle $\pm\alpha_{ss}$ at $Re = 1.15 \times 10^5$.

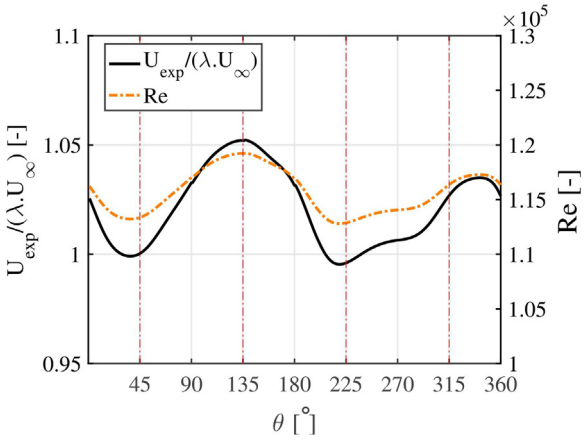

Fig. 16. Non-dimensional experienced velocity and local chord-based Reynolds number during a revolution at β = 0°.

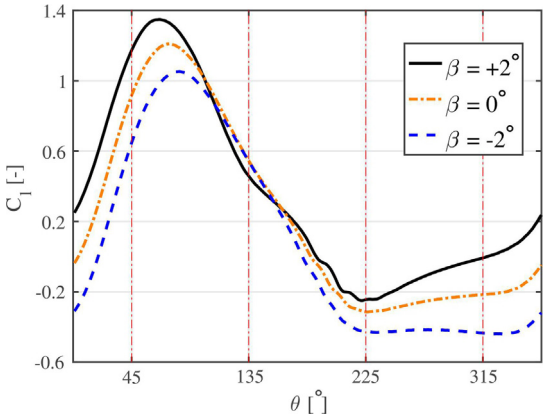

Fig. 17. Dynamic lift coefficient versus azimuth for β = +2°, 0° and −2° for the last revolution of the turbine.

are a result of blade-wake interaction: the blades in the downwind area travel through the vortices shed by the blades on the upwind side. Moreover, the effect of asymmetry in the wake is also observed as a slope in α on the downwind side; this effect is more pronounced for β > −2° where there is a decreasing trend in the absolute value of α on the downwind side from θ = 225° to 315°. This is consistent with the asymmetry in the wake, which is found to be towards the windward side for such β (cf. Fig. 13c).

The variation of the experienced velocity and local chord-based Reynolds number (Re) for a blade of the turbine over a revolution at zero pitch angle (see Fig. 16) shows that the experienced velocity for the turbine has an approximately sinusoidal oscillation with a peak-to-peak amplitude of 5% over each revolution where the period is half a revolution. The highest (lowest) values occur at θ ≈ 135° and 315° (θ ≈ 45° and 225°).

6.2.2. Dynamic loads on the blades

Among the studied fixed pitch angles, three values of β = +2°, 0° and −2° are selected to elucidate the effect of pitch angle on the dynamic loads on an unsteady airfoil, the boundary layer events (Section 6.2.3), the pressure coefficient distribution on the airfoil (Section 6.2.4) and the shed vorticity (Section 6.2.5). The variation of C_l of the unsteady airfoil versus azimuth shows a similar trend as α (Fig. 17). The similarity is in agreement with results obtained by Moore [73] for harmonic variations of α for a pitching airfoil: the variation in α for 0° ≤ θ ≤ 180° is almost harmonic while it is less regular for 180° < θ ≤ 360°. A more or less monotonic trend is observed for 225° ≤ θ ≤ 345°.

The reduced frequency (K) is typically used to determine the level of unsteadiness for unsteady airfoils which for the present VAWT, calculated using Eq. (5) below, is 0.058.

$$K = \frac{\Omega c}{2U_{\text{exp}}} \tag{5}$$

Comparing Fig. 17 with Fig. 15 it is observed that the maximum lift coefficient $C_{l,max}$ for the unsteady airfoil happens at an earlier azimuthal position than α_{max}. This is in line with experimental observations of Lee and Gerontakos [70] at similar reduced frequencies (K ≈ 0.05) where they tested the thinner NACA0012 airfoil under pitching motion (below, near or in light and deep stall). Increasing β is found to slightly shift the azimuthal position of $C_{l,max}$ to smaller values which is caused by the higher α_{max}.

Variations of the lift and drag coefficients (C_l and C_d) versus α show a large hysteresis for the dynamic loads (see Fig. 18). It is observed that for α > 0° the hysteresis increases for larger β: this is due to higher α_{max} experienced by the blade. The opposite effect is observed for α < 0. Moreover, it is found that the slope of the C_l-α curve increases (decreases) with increasing (decreasing) α, leading to an increasing difference with static airfoil values. The findings correspond with those for pitching airfoils [70,71] where this is found to be a result of a higher resistance of the boundary layer to separation (due to its fuller velocity profile) during the upstroke, and a consequent delay in separation at similar reduced frequencies (K ≈ 0.05) and for situations near or in light stall. The upstroke

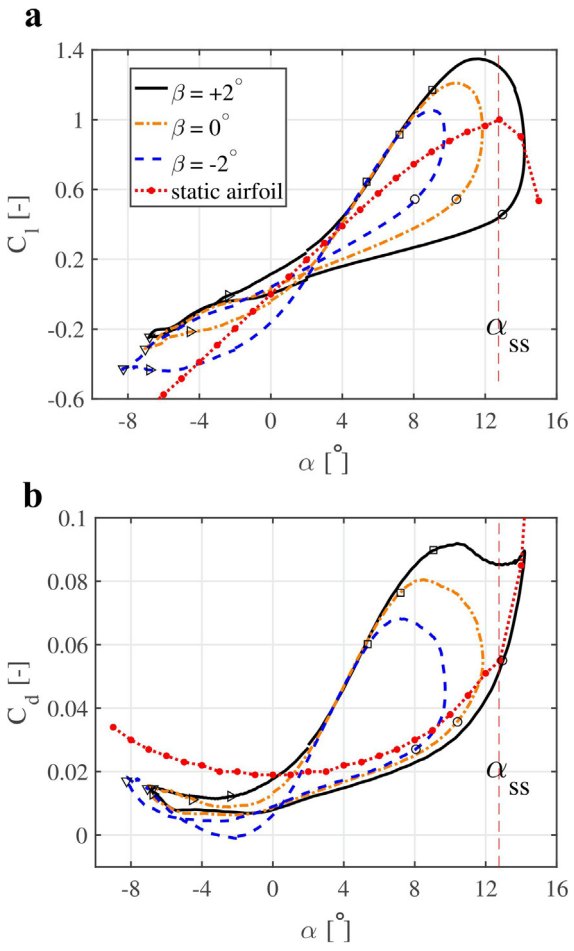

Fig. 18. (a) Lift and (b) drag coefficients versus angle of attack for the dynamic and static airfoil; □, θ = 45°; ○, θ = 135°; ▽, θ = 225°; ▷, θ = 315°; *arrow:* direction based on the revolution of the turbine.

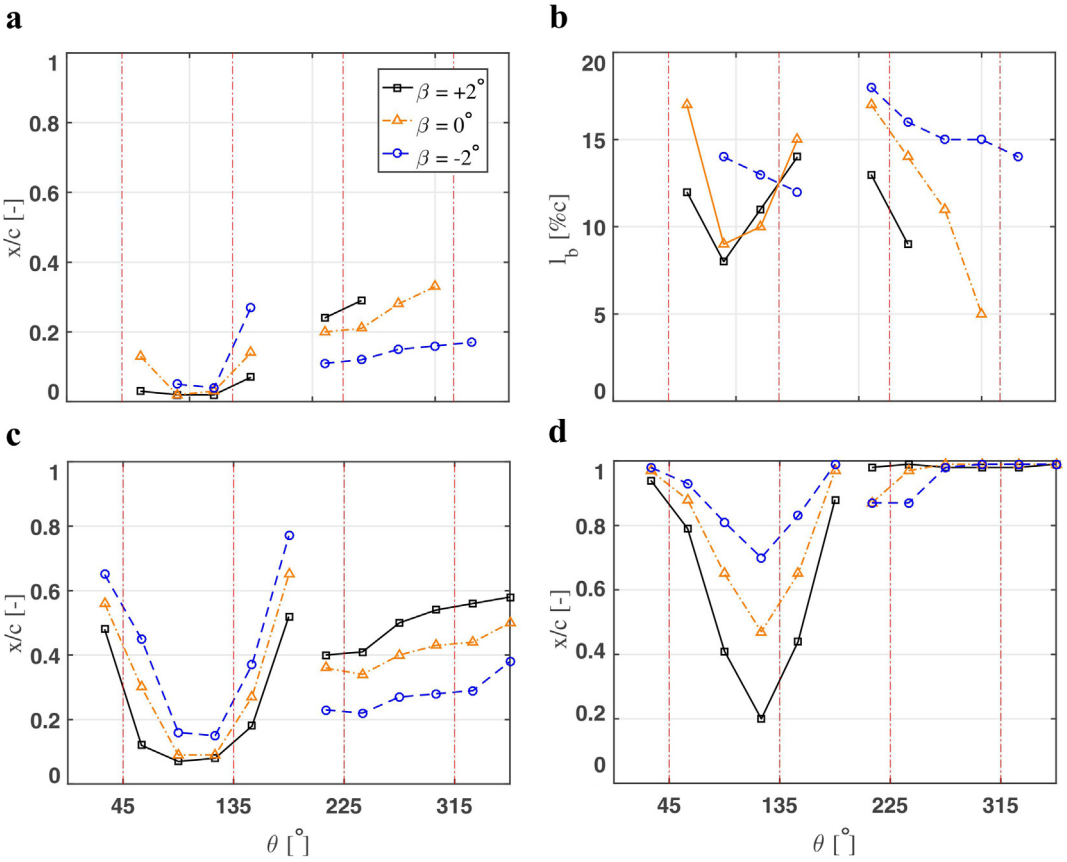

Fig. 19. Critical boundary layer events on the suction side of the airfoil versus azimuth: (a) laminar separation point; (b) bubble length l_b; (c) peak transition point, (d) trailing edge turbulent separation point.

(where the trailing edge separation point moves upstream toward the leading edge) resembles the case of a downstream-moving wall [71]. The situation is reversed for the downstroke (decreasing α) where separation is provoked compared to the static airfoil and a lower slope of the C_l-α curve is observed than in the static case. The observed behavior for the unsteady airfoil of the VAWT and the similarity with the pitching airfoil implies that the variation in α is the dominant source of flow unsteadiness for a VAWT, not the time-dependent experienced velocity.

The $C_{l,max}$ for the unsteady airfoil is much higher than the corresponding static value. This difference is found to be a result of the delay in boundary layer events (transition to turbulence and separation) for $\alpha_u < \alpha_{ss}$ [70]. The same physical process explains the higher values of C_l for the given value of α_u compared to the static airfoil. Higher C_l values than those for the static airfoil are observed even at small angles of attack: the point where both curves depart corresponds to the position where the trailing edge separation point starts to move upstream (see Section 6.2.3). The reverse applies for α_d which results in lower values of C_l for the given α_d. The loads do not return to static values until the angle of attack decreases to very small values and the flow is reattached on large parts of the suction side; the trailing edge turbulent separation persists during the whole revolution while covering only 1–3% of the chord in the downwind area (see Section 6.2.3). It is observed that the value of α at which $C_{l,max}$ occurs for the unsteady airfoil with $\beta = +2°$ (where $\alpha_{max} > \alpha_{ss}$) is lower than that of the static airfoil, in contrast with the trend observed for pitching airfoils [70]. This might be a result of the time-dependent incoming flow which is known to promote separation [71].

These comparisons highlight that unsteady airfoil data even for small variations in β, where α_{max} is below or slightly higher than α_{ss}, are very different from static airfoil data. As a result, application of the inviscid theory does not result in correct loads and moments on the blades.

6.2.3. Boundary layer events

Boundary layer event locations (leading edge laminar separation, laminar-to-turbulent transition and trailing edge turbulent separation points) on the suction side of the airfoil during the revolution of the turbine are plotted versus azimuth (Fig. 19) and angle of attack (Fig. 20) for pitch angles $\beta = +2°$, 0° and −2°. Note that the suction side is on the inner side for approximately $0° \leq \theta \leq 180°$ and on the outer side for approximately $180° < \theta < 360°$.

It is observed that a laminar separation bubble develops near the leading edge on the suction side; the bubble moves upstream (downstream) with increasing (decreasing) α. The bubble length is 5–20% of the airfoil chord during the revolution with a tendency of the bubble length to decrease (increase) with increasing (decreasing) angle of attack. Similar trends for the laminar separation point location and bubble length are experimentally observed by Lee and Gerontakos [70]. Higher values for β are found to result in higher (lower) α for $0° \leq \theta \leq 180°$ ($180° < \theta < 360°$), as a result of which laminar separation occurs closer to (farther from) the leading edge compared to zero pitch angle.

For angles of attack where the laminar separation bubble is present it serves to transition the flow from laminar to turbulent. The laminar-to-turbulent transition process in the laminar separation bubble has been found to occur through instabilities in the shear layer over the bubble [74]. The transition peak location moves upstream (downstream) with increasing (decreasing) α. Turbulent trailing edge separation persists during the revolution on the suction side but only occurs at $\theta \approx 180°$ on the pressure side. The

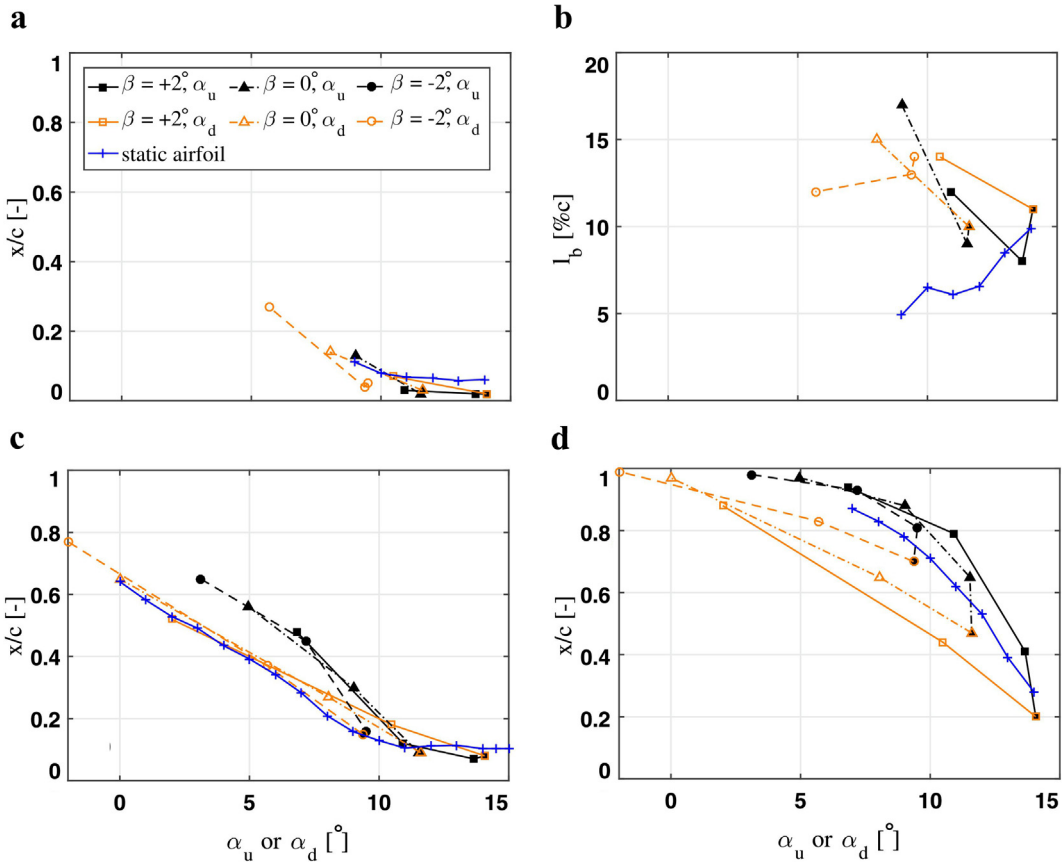

Fig. 20. Critical boundary layer events on the suction side of the airfoil versus α for $0° \leq \theta \leq 180°$: (a) laminar separation point; (b) bubble length l_b; (c) peak transition point; (d) trailing edge turbulent separation point.

trailing edge separation location follows a similar trend as the transition peak location: it moves upstream (downstream) with increasing (decreasing) α where the rate of movement of the trailing edge separation point is more sensitive to α than the transition peak location. These findings are in agreement with results for pitching airfoils [70,71,74]. Additionally, higher (lower) β are found to shift the transition and trailing-edge separation points upstream (downstream) for the fore half of the turbine ($0° \leq \theta \leq 180°$) whereas the reverse applies for the aft half ($180° < \theta < 360°$). Wind tunnel tuft visualizations by Armstrong et al. [51] similarly reported a delay in separation for lower β.

Hysteresis is found (Fig. 20) for the laminar separation point, bubble length, and laminar-to-turbulent transition and trailing edge turbulent transition points. The asymmetry between upstroke and downstroke is much stronger for the trailing edge separation than for other boundary layer events; this is consistent with its higher sensitivity to α pointed out earlier in this section. The hysteresis in the boundary layer events and the effect of pitch angle correlate well with the hysteresis observed in dynamic loads on the airfoil (Fig. 18). Higher β values are found to increase the hysteresis. The increase in asymmetry for higher β is found to be due to larger α_{max} experienced by the airfoil during the revolution. These findings are consistent with observations for pitching airfoils at similar reduced frequencies [70,71,74]. The speed at which the trailing edge separation point moves upstream (downstream) is also found to increase with increasing α_{max}. The speed of the upstream (downstream) movement of leading edge separation and transition peak locations shows a similar trend but it is less sensitive to α_{max}.

6.2.4. Pressure coefficient distributions on the blades

The boundary layer events can also be inferred to some extent from the pressure distributions on the blades. A sudden increase in the rate of pressure recovery signals the point of laminar separation and the pressure gradient will remain approximately zero over the separation bubble. A sudden increase in pressure then indicates the transition peak location and the second sudden decrease in rate of pressure recovery signals the reattachment point [72,75]. The boundary layer events presented in Section 6.2.3 could all be confirmed from the pressure distribution over the suction side of the airfoil in this way. The distribution of pressure coefficient (CoP) along the suction and pressure sides of the airfoil for different pitch angles $\beta = 0°$, $+2°$ and $-2°$ are compared at selected azimuthal positions in Fig. 21. These positions are selected to further highlight the effect of pitch angle on CoP. Compared to zero pitch a pitch angle of $\beta = +2°$ results in more negative CoP on the suction side and more positive CoP on the pressure side of the airfoil on the upwind part (for $\theta = 40°$, $70°$ and $90°$); a similar trend is observed for $\beta = -2°$ on the downwind and windward sides (for $\theta = 240°$, $280°$, $320°$ and $360°$). This is consistent with the moment coefficients on the blades shown in Fig. 12a.

6.2.5. Wake generation

To further clarify the effect of pitch angle on the aerodynamics of a VAWT, the strength of the shed vorticity by a single VAWT blade during the revolution is compared for pitch angles $\beta = 0°$, $+2°$ and $-2°$. It is calculated by equating two definitions for the lift force (one based on the lift coefficient and the other based on the Kutta–Joukowski theorem [76]) where the anti-clockwise direction

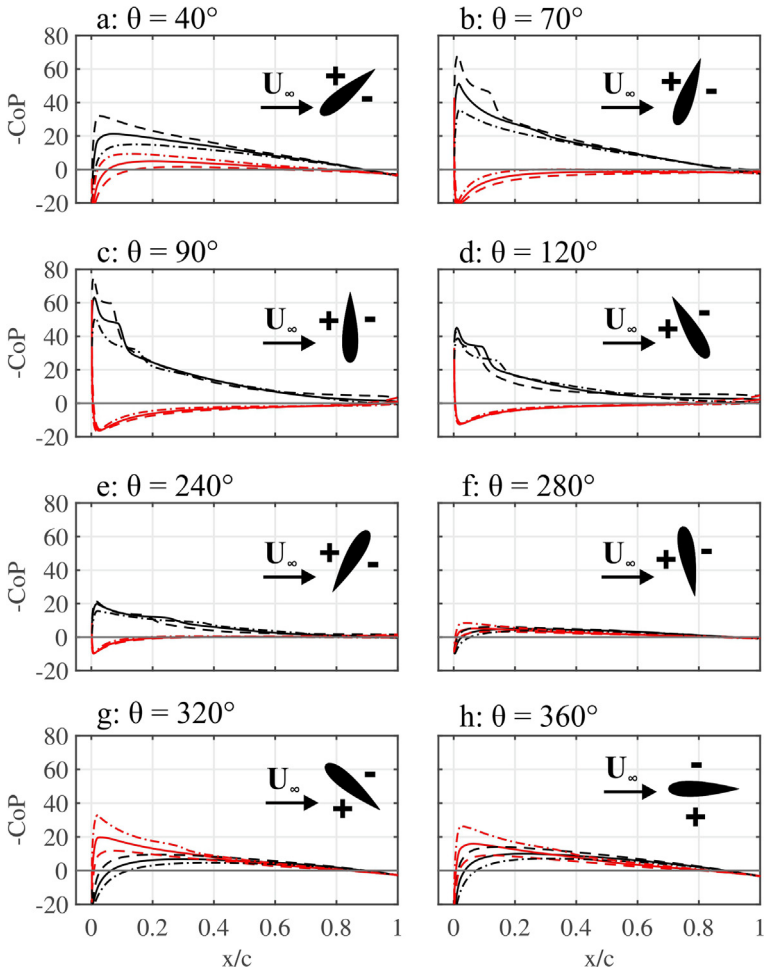

Fig. 21. Pressure coefficient distribution for outer (red) and inner (black) sides of the airfoil at different azimuthal positions during the last revolution for different pitch angles: β = 0° (solid line), β = +2° (dashed line), β = −2° (dash-dot line): pressure side (+), suction side (−). (For interpretation of the references to colour in this figure legend, the reader is referred to the web version of this article.)

around z-axis is positive. The rate of change in circulation per degree azimuth ($\frac{\partial\Gamma}{\partial\theta}$) is equal to the strength of the shed vorticity by a single VAWT blade during the revolution (see Eq. (6)) which in non-dimensional form is provided in Eq. (7) [11].

$$\frac{\partial\Gamma}{\partial\theta} = -0.5U_\infty c\frac{\partial C_l}{\partial\theta} \tag{6}$$

$$\frac{2}{cU_\infty}\frac{\partial\Gamma}{\partial\theta} = -\frac{\partial C_l}{\partial\theta} \tag{7}$$

The comparison (see Fig. 22) shows that introducing the pitch angle can create a significant difference in wake generation, especially in the upwind and downwind parts of the turbine revolution, while the overall trend as a function of azimuthal position remains similar. This means that adding a fixed bound circulation to the airfoil (i.e. fixed pitch angle) not only changes the instantaneous loads and moments on the blades but also the average loading during the revolution and consequently the power. This is consistent with the change in C_P as a function of pitch angle observed in Fig. 13a but in contradiction with the inviscid findings of Simão Ferreira and Scheurich [11].

7. Discussion

The effect of stalled flow on the VAWT blade for β = +3° is visible for both instantaneous (C_m, C_{Fx}, C_{Fy} and C_{Fn}) and averaged (C_P and C_T) loading on blades. This is seen as a sudden drop in moment and thrust force and the following ripples in the instantaneous values which is due to the inherent unsteadiness of the stalled flow. The occurrence of stall is also observed in the variations of angle of attack where α_{max} far exceeds α_{ss}. For β = −7° it is also observed that α_{max} exceeds $-\alpha_{ss}$ in the downwind region and further

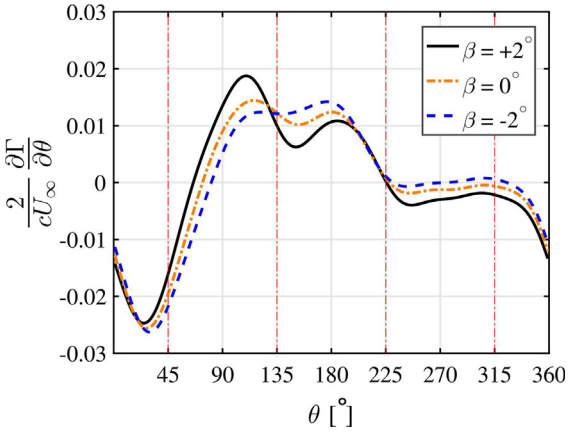

Fig. 22. Shed vorticity of one blade for the last revolution versus azimuth for β = +2°, 0° and −2° where (+) denotes counter-clockwise circulation based on the Kutta–Joukowski theorem [76].

decrease in pitch angle might lead to stall. Occurrence of stall and the consequent power loss and unsteadiness in loads sets the limit for adjusting the maximum (minimum) pitch angle on the blades.

An optimum fixed pitch angle of $-2°$ is found to improve the performance of the turbine by 6.6%. This means that setting an optimum fixed pitch angle can be an effective method to enhance VAWT performance which is in contrast with results of Simão Ferreira and Scheurich [11] where pitch angle was found to have insignificant influence for improvement of the performance of the turbine. However, the fact that the optimum fixed pitch angle leads to higher C_m during only part of the revolution while decreased C_m is observed elsewhere implies that different operational (λ) or geometrical parameters (airfoil shape) might lead to a different optimum fixed value for β, and that the value needs to be determined for each design. This also means that even no pitch ($\beta = 0°$) might be optimal under some conditions. The main intention of the present study is to highlight the influence of the pitch angle on instantaneous and averaged loading of a VAWT as well as the associated aerodynamics, and to further advance knowledge on the effectiveness of pitch angle as a parameter for improvement of aerodynamic efficiency of VAWTs. In addition, the provided conclusions aim to contribute to research on optimal dynamic pitching as a promising power enhancement option for such turbines. It is known that different operational and geometrical characteristics of the turbine might result in a different optimal pitch angle which limits the generality of the absolute value of optimal pitch angle identified in the current study. Indeed, Future research is proposed to generalize the identification of optimal pitch angle values under various operational and geometrical conditions, mainly different airfoil shapes typically used for VAWTs.

For both the instantaneous moment coefficient and x-force coefficient a shift between fore ($0° \leq \theta \leq 180°$) and aft ($180° < \theta < 360°$) halves of the revolution is observed for increasing pitch angle. Positive pitch angles are more favorable mainly in the fore half of the turbine rotation while the reverse applies for negative pitch angles. An approximately similar shift between the upwind and downwind regions of the turbine as a result of changing β is observed for the pressure difference on the blade and the strength of the shed vortices. This is consistent with the variations observed for the angle of attack and lift coefficient where positive β results in higher $|\alpha|$ and $|C_l|$ for the fore half and negative β results in higher $|\alpha|$ and $|C_l|$for the aft half of the revolution. The shift in the instantaneous y-force coefficient (C_{FY}) is between the top ($270° < \theta \leq 360°$ and $0° < \theta < 90°$) and bottom ($90° \leq \theta \leq 270°$) halves of the revolution. No shift is observed in the instantaneous coefficient of normal force (C_{Fn}). A similar shift in the instantaneous loads and moments was previously observed in inviscid results by Simão Ferreira and Scheurich [11]. The observed shift in the key parameters of the turbine suggests that although setting a fixed value of pitch angle might be beneficial for the turbine, the potential gain from a variable pitching blade can be significantly higher. This is therefore a promising topic for future research.

The findings of the current study support improvement of the aerodynamic performance of VAWTs in the following ways:

- The results show that an optimum fixed pitch angle can improve the performance of VAWT by more than 5% compared to zero pitch. This finding is important as introducing a fixed pitch to the blade is practically very simple and inexpensive. Furthermore the physical processes underlying the effect on turbine performance are analyzed in detail. Future research is proposed to investigate optimum pitch angles for other tip speed ratios.
- The presented instantaneous moment coefficients of the turbine blades under the influence of fixed pitch angle provides essential information for further improvement of aerodynamic performance of VAWTs using optimal dynamic pitching, where a first estimate of the optimum pitch distribution for each blade can be derived from the distribution of C_m with fixed pitch angle. The presented results imply that optimal dynamic pitching might be a very promising strategy for enhancement of VAWT performance due to the variations of angle of attack on the blades during each revolution. Future research is recommended to further investigate this topic.
- The presented results and discussions on the effect of pitch angle on boundary layer events (leading-edge and trailing-edge separation, laminar separation bubble length and laminar-to-turbulent transition) increase physical understanding of the effect of pitch angle on turbine performance which is highly useful for turbine design. For example, this information can be used to support the application of flow control mechanisms to locally manipulate the flow on blades of VAWTs to achieve the desired conditions, namely postponing flow separation, controlling the circulation around the airfoil and transition control. Optimal performance of VAWT could be achieved via transient local control of flow on each individual blade during the revolution.

8. Conclusions

The effect of fixed pitch angle β on the loads and moments as well as the aerodynamics of a 3-bladed VAWT have been studied using URANS calculations with transition SST turbulence modeling. The main conclusions are:

- Due to variations in α during the revolution, different β values result in higher C_m only over a small part of the revolution. $\beta > 0°$ is found to be optimal for $25° < \theta < 90°$ while $\beta < 0°$ produces higher C_m for $0° < \theta < 25°$ and $90° < \theta < 360°$. This suggests a high potential for VAWT performance improvement using variable angle blade pitching.
- For the studied turbine $\beta = -2°$ is found to be optimal, with a 6.6% (2%) higher C_P (C_T) compared to $\beta = 0°$. Moreover, it results in an approximately symmetric wake ($C_Y \approx 0$) while the wake has a windward asymmetry for $\beta = 0°$.
- $\beta = +3°$ is found to result in a large drop in C_P due to stall on blades in the upwind area.
- Changing β shifts the instantaneous loads and moments on the blades between fore ($0° \leq \theta \leq 180°$) and aft ($180° < \theta < 360°$) halves of the revolution for C_m and C_{FX} and between the top ($270° < \theta < 360$ and $0° < \theta < 90°$) and bottom ($90° \leq \theta \leq 270°$) halves for C_{FY}. No shift is observed in the instantaneous coefficient of normal force (C_{Fn}).
- Variations in experienced angle of attack and velocity are shown as two sources of flow unsteadiness for a VAWT where the former is identified as the major contributor to the behavior of critical boundary layer events on the blades. It is observed that for $\beta = +2°$, $+3°$ and $-7°$, α exceeds the static stall angle α_{ss}. However, the occurrence of stall is only observed for $\beta = +3°$. The higher resistance to flow separation of the boundary layer on an airfoil with increasing angle of attack is found to delay stall on the blades: as a result it does not occur for $\beta = +2°$ and $-7°$ although $\alpha > \pm\alpha_{ss}$.
- A large hysteresis is found for dynamic loads on the blades as well as for the boundary layer events (leading edge laminar separation, laminar-to-turbulent transition and trailing edge turbulent separation points). $C_{l,max}$ is found to reach much higher values than the corresponding static value and the slope of the C_l-α curve is found to be larger (smaller) than the static value during the upstroke (downstroke). This is due to delayed

separation during the upstroke as a result of higher resistance to separation of the boundary layer, which in turn is caused by its fuller velocity profile. The reverse applies for the downstroke.

- The hysteresis (asymmetry) increases for higher β due to higher experienced α_{max} during the revolution.
- Laminar-to-turbulent transition and trailing edge separation point locations are found to move upstream (downstream) with increasing (decreasing) α. The trailing edge separation persists on the suction side throughout the revolution. The effect of higher (lower) β is similar to a shift in α to higher (lower) values.
- The pitch angle affects the strength of the shed vorticity by the VAWT blade whereas the trend as a function of azimuthal position remains similar. This means that adding a fixed bound circulation on the blade can change the instantaneous loads and moments on the blades as well as the wake generation, power conversion and average loading.

Acknowledgements

The authors would like to acknowledge support from the European Commission's Framework Program Horizon 2020, through the Marie Curie Innovative Training Network (ITN) AEOLUS4FUTURE - Efficient harvesting of the wind energy (H2020-MSCA-ITN-2014: Grant agreement no. 643167) and the TU1304 COST ACTION "WINERCOST". The authors gratefully acknowledge the partnership with ANSYS CFD. This work was sponsored by NWO Exacte Wetenschappen (Physical Sciences) for the use of supercomputer facilities, with financial support from the Nederlandse Organisatie voor Wetenschappelijk Onderzoek (Netherlands Organization for Scientific Research, NWO).

References

[1] Zeiner-Gundersen DH. A novel flexible foil vertical axis turbine for river, ocean, and tidal applications. Appl Energy 2015;151:60–6.
[2] Borg M, Collu M. Frequency-domain characteristics of aerodynamic loads of offshore floating vertical axis wind turbines. Appl Energy 2015;155:629–36.
[3] Bedon G, Schmidt Paulsen U, Aagaard Madsen H, Belloni F, Raciti Castelli M, Benini E. Computational assessment of the DeepWind aerodynamic performance with different blade and airfoil configurations. Appl Energy 2017;185:1100–8.
[4] Balduzzi F, Bianchini A, Carnevale EA, Ferrari L, Magnani S. Feasibility analysis of a darrieus vertical-axis wind turbine installation in the rooftop of a building. Appl Energy 2012;97:921–9.
[5] Yang A-S, Su Y-M, Wen C-Y, Juan Y-H, Wang W-S, Cheng C-H. Estimation of wind power generation in dense urban area. Appl Energy 2016;171:213–30.
[6] Li QS, Shu ZR, Chen FB. Performance assessment of tall building-integrated wind turbines for power generation. Appl Energy 2016;165:777–88.
[7] Paraschivoiu I. Wind turbine design: with emphasis on darrieus concept. Montréal, Québec: Polytechnic International Press; 2009.
[8] Sutherland HJ, Berg DE, Ashwill TD. A retrospective of VAWT technology," Sandia National Laboratories; 2012.
[9] Tummala A, Velamati RK, Sinha DK, Indraja V, Krishna VH. A review on small scale wind turbines. Renew Sustain Energy Rev 2016;56:1351–71.
[10] Simão Ferreira C, Geurts B. Aerofoil optimization for vertical-axis wind turbines. Wind Energy 2014;18(8):1371–85.
[11] Simão Ferreira C, Scheurich F. Demonstrating that power and instantaneous loads are decoupled in a vertical-axis wind turbine. Wind Energy 2014;17(3):385–96.
[12] Simão Ferreira C, Hofemann C, Dixon K, van Kuik G, van Bussel G. 3D wake dynamics of the VAWT: experimental and numerical investigation. In: 48th AIAA aerospace sciences meeting including the new horizons forum and aerospace exposition, Orlando, Florida, 4–7 Jan. 2010.
[13] Tescione G, Ragni D, He C, Simão Ferreira C, van Bussel GJW. Near wake flow analysis of a vertical axis wind turbine by stereoscopic particle image velocimetry. Renew Energy 2014;70:47–61.
[14] Simão Ferreira C, van Kuik G, van Bussel G, Scarano F. Visualization by PIV of dynamic stall on a vertical axis wind turbine. Exp Fluids 2008;46(1):97–108.
[15] Schuerich F, Brown RE. Effect of dynamic stall on the aerodynamics of vertical-axis wind turbines. AIAA J 2011;49(11):2511–21.
[16] Migliore PG, Wolfe WP, Fanucci JB. Flow curvature effects on Darrieus turbine blade aerodynamics. J Energy 1980;4(2):49–55.
[17] Bianchini A, Balduzzi F, Ferrara G, Ferrari L. Virtual incidence effect on rotating airfoils in Darrieus wind turbines. Energy Convers Manage 2016;111:329–38.
[18] Chehouri A, Younes R, Ilinca A, Perron J. Review of performance optimization techniques applied to wind turbines. Appl Energy 2015;142:361–88.
[19] Islam M, Ting D, Fartaj A. Aerodynamic models for Darrieus-type straight-bladed vertical axis wind turbines. Renew Sustain Energy Rev 2008;12(4):1087–109.
[20] Simão Ferreira C, Madsen HA, Barone M, Roscher B, Deglaire P, Arduin I. Comparison of aerodynamic models for vertical axis wind turbines. J Phys: Conf Ser 2014;524(012125).
[21] Wang L, Yeung RW. On the performance of a micro-scale Bach-type turbine as predicted by discrete-vortex simulations. Appl Energy 2016;183:823–36.
[22] Balduzzi F, Bianchini A, Maleci R, Ferrara G, Ferrari L. Critical issues in the CFD simulation of Darrieus wind turbines. Renew Energy 2016;85:419–35.
[23] Chen W-H, Chen C-Y, Huang C-Y, Hwang C-J. Power output analysis and optimization of two straight-bladed vertical-axis wind turbines. Appl Energy 2017;185:223–32.
[24] Danao LA, Edwards J, Eboibi O, Howell R. A numerical investigation into the influence of unsteady wind on the performance and aerodynamics of a vertical axis wind turbine. Appl Energy 2014;116:111–24.
[25] Blocken B. Computational fluid dynamics for urban physics: Importance, scales, possibilities, limitations and ten tips and tricks towards accurate and reliable simulations. Build Environ 2015;91:219–45.
[26] Blocken B. 50 years of computational wind engineering: past, present and future. J Wind Eng Ind Aerodynam 2014;129:69–102.
[27] Rezaeiha A, Kalkman IM, Blocken B. CFD simulation of a vertical axis wind turbine operating at a moderate tip speed ratio: guidelines for minimum domain size and azimuthal increment. Renew Energy 2017;107:373–85.
[28] Araya DB, Dabiri JO. A comparison of wake measurements in motor-driven and flow-driven turbine experiments. Exp Fluids 2015;56(7).
[29] Scungio M, Arpino F, Focanti V, Profili M, Rotondi M. Wind tunnel testing of scaled models of a newly developed Darrieus-style vertical axis wind turbine with auxiliary straight blades. Energy Convers Manage 2016;130:60–70.
[30] Pagnini LC, Burlando M, Repetto MP. Experimental power curve of small-size wind turbines in turbulent urban environment. Appl Energy 2015;154:112–21.
[31] Rolland SA, Thatcher M, Newton W, Williams AJ, Croft TN, Gethin DT, et al. Benchmark experiments for simulations of a vertical axis wind turbine. Appl Energy 2013;111:1183–94.
[32] Klimas PC, Worstell M. Effects of blade preset pitch/offset on curved-blade Darrieus vertical axis wind turbine performance. USA: Sandia National Laboratories; 1981.
[33] Simão Ferreira C, Barone MF, Zanon A, Kemp R, Giannattasio P. Airfoil optimization for stall regulated vertical axis wind turbines. In: 33rd wind energy symposium, Kissimmee, Florida, 5–9 Jan. 2015.
[34] Lin S-Y, Lin Y-Y, Bai C-J, Wang W-C. Performance analysis of vertical-axis-wind-turbine blade with modified trailing edge through computational fluid dynamics. Renew Energy 2016;99:654–62.
[35] Bedon G, De Betta S, Benini E. Performance-optimized airfoil for Darrieus wind turbines. Renew Energy 2016;94:328–40.
[36] Li Q, Maeda T, Kamada Y, Murata J, Shimizu K, Ogasawara T, et al. Effect of solidity on aerodynamic forces around straight-bladed vertical axis wind turbine by wind tunnel experiments (depending on number of blades). Renew Energy 2016;96:928–39.
[37] Bianchini A, Ferrara G, Ferrari L. Pitch optimization in small-size Darrieus wind turbines. Energy Proc 2015;81:122–32.
[38] Rezaeiha A, Kalkman IM, Blocken B. Effect of the shaft on the aerodynamic performance of an urban vertical axis wind turbine: a numerical study; 2017 [submitted for publication].
[39] Parker CM, Leftwich MC. The effect of tip speed ratio on a vertical axis wind turbine at high Reynolds numbers. Exp Fluids 2016;57(5).
[40] Wekesa DW, Wang C, Wei Y, Zhu W. Experimental and numerical study of turbulence effect on aerodynamic performance of a small-scale vertical axis wind turbine. J Wind Eng Ind Aerodynam 2016;157:1–14.
[41] Danao LA, Eboibi O, Howell R. An experimental investigation into the influence of unsteady wind on the performance of a vertical axis wind turbine. Appl Energy 2013;107:403–11.
[42] Lazauskas L. Three pitch control systems for vertical axis wind turbine. Wind Eng 1992;16(5):269–82.
[43] Paraschivoiu I, Trifu O, Saeed F. H-Darrieus wind turbine with blade pitch control. Int J Rotating Mach 2009;2009:1–7.
[44] Soraghan CE, Leithead WE, Feuchtwang J, Yue H. Double multiple streamtube model for variable pitch vertical axis wind turbines. In: 31st AIAA Applied Aerodynamics Conference, San Diego, CA, 24–27 Jun. 2013.
[45] Jain P, Abhishek A. Performance prediction and fundamental understanding of small scale vertical axis wind turbine with variable amplitude blade pitching. Renew Energy 2016;97:97–113.
[46] Hwang IS, Lee YH, Kim SJ. Optimization of cycloidal water turbine and the performance improvement by individual blade control. Appl Energy 2009;86(9):1532–40.
[47] Chen C-C, Kuo C-H. Effects of pitch angle and blade camber on flow characteristics and performance of small-size Darrieus VAWT. J Vis 2012;16(1):65–74.
[48] Zhang L-X, Liang Y-B, Liu X-H, Guo J. Effect of blade pitch angle on aerodynamic performance of straight-bladed vertical axis wind turbine. J Central South Univ 2014;21(4):1417–27.

[49] Bose Surmantraa R, Chandramouli S, Premsai TP, Prithviraj P, Vivek M, Ratna Kishore V. Numerical analysis of effect of pitch angle on a small scale vertical axis wind turbine. Int J Renew Energy Res 2014;4(4):929–35.
[50] Fiedler AJ, Tullis S. Blade offset and pitch effects on a high solidity vertical axis wind turbine. Wind Eng 2009;33(3):237–46.
[51] Armstrong S, Fiedler A, Tullis S. Flow separation on a high Reynolds number, high solidity vertical axis wind turbine with straight and canted blades and canted blades with fences. Renew Energy 2012;41:13–22.
[52] Benedict M, Lakshminarayan V, Pino J, Chopra I. Aerodynamics of a small-scale vertical-axis wind turbine with dynamic blade pitching. AIAA J 2016;54 (3):924–35.
[53] Liang Y-B, Zhang L-X, Li E-X, Zhang F-Y. Blade pitch control of straight-bladed vertical axis wind turbine. J Central South Univ 2016;23(5):1106–14.
[54] Erickson D, Wallace J, Peraire J. Performance characterization of cyclic blade pitch variation on a vertical axis wind turbine. In: 49th AIAA aerospace sciences meeting including the new horizons forum and aerospace exposition, Orlando, Florida, 4–7 Jan. 2011.
[55] Elkhoury M, Kiwata T, Aoun E. Experimental and numerical investigation of a three-dimensional vertical-axis wind turbine with variable-pitch. J Wind Eng Ind Aerodynam 2015;139:111–23.
[56] Kinzel M, Maughmer MD, Duque EPN. Numerical investigation on the aerodynamics of oscillating airfoils with deployable Gurney flaps. AIAA J 2010;48(7):1457–69.
[57] Roache PJ. Quantification of uncertainty in computational fluid dynamics. Ann Rev Fluid Mech 1997;29:123–60.
[58] ANSYS. ANSYS® Fluent theory guide, release 16.1, ANSYS Inc; 2015.
[59] Menter FR, Langtry RB, Likki SR, Suzen YB, Huang PG, Völker S. A correlation-based transition model using local variables—part I: model formulation. J Turbomach 2006;128(3):413–22.
[60] Langtry RB, Menter FR, Likki SR, Suzen YB, Huang PG, Völker S. A correlation-based transition model using local variables—part II: test cases and industrial applications. J Turbomach 2006;128(3):423–34.
[61] Blocken B, Stathopoulos T, Carmeliet J. CFD simulation of the atmospheric boundary layer: wall function problems. Atmos Environ 2007;41(2): 238–52.
[62] Blocken B, Carmeliet J, Stathopoulos T. CFD evaluation of wind speed conditions in passages between parallel buildings—effect of wall-function roughness modifications for the atmospheric boundary layer flow. J Wind Eng Ind Aerodynam 2007;95(9–11):941–62.
[63] Aslam Bhutta MM, Hayat N, Farooq AU, Ali Z, Jamil SR, Hussain Z. Vertical axis wind turbine – a review of various configurations and design techniques. Renew Sustain Energy Rev 2012;16(4):1926–39.
[64] Islam MR, Mekhilef S, Saidur R. Progress and recent trends of wind energy technology. Renew Sustain Energy Rev 2013;21:456–68.
[65] Tjiu W, Marnoto T, Mat S, Ruslan MH, Sopian K. Darrieus vertical axis wind turbine for power generation I: assessment of Darrieus VAWT configurations. Renew Energy 2015;75:50–67.
[66] Simão Ferreira C. The near wake of the VAWT: 2D and 3D views of the VAWT aerodynamics. PhD, TU Delft; 2009.
[67] Shen WZ, Hansen MOL, Sørensen JD. Determination of the angle of attack on rotor blades. Wind Energy 2009;12:91–8.
[68] Richardson LF. The approximate arithmetical solution by finite differences of physical problems involving differential equations, with an application to the stresses in a masonry dam. Philos Trans Roy Soc Lond Ser A, Contain Pap Math Phys Character 1911;210(459–470):307–57.
[69] Castelli MR, Englaro A, Benini E. The Darrieus wind turbine: proposal for a new performance prediction model based on CFD. Energy 2011;36(8):4919–34.
[70] Lee T, Gerontakos P. Investigation of flow over an oscillating airfoil. J Fluid Mech 2004;512:313–41.
[71] Gad-el-Hak M, Bushnell DM. Separation control: review. J Fluids Eng 1991;113 (1):5–30.
[72] O'Meara M, Mueller TJ. Laminar separation bubble characteristics on an airfoil at low Reynolds numbers. AIAA J 1987;25(8):1033–41.
[73] Moore FK. Lift hysteresis at stall as an unsteady boundary-layer phenomenon. NASA, Cleveland, OH, United States NACA-TR-1291; 1993.
[74] Nati A, de Kat R, Scarano F, van Oudheusden BW. Dynamic pitching effect on a laminar separation bubble. Exp Fluids 2015;56(9).
[75] Tani I. Low-speed flows involving bubble separations. Prog Aerospace Sci 1964;5(C):70–103.
[76] Anderson JD. Fundamental of aerodynamics. Boston: McGraw-Hill; 2001.